# Synthetic riboswitches for the analysis of tRNA processing by eukaryotic RNase P enzymes

ANNA ENDER,[1,6] NADINE GRAFL,[1,6] TIM KOLBERG,[1] SVEN FINDEIß,[2] PETER F. STADLER,[2,3,4,5] and MARIO MÖRL[1]

[1]Institute for Biochemistry, Leipzig University, 04103 Leipzig, Germany
[2]Bioinformatics Group, Department of Computer Science and Interdisciplinary Center for Bioinformatics, Leipzig University, 04107 Leipzig, Germany
[3]Max Planck Institute for Mathematics in the Science, 04103 Leipzig, Germany
[4]Institute for Theoretical Chemistry, University of Vienna, A-1090 Vienna, Austria
[5]Santa Fe Institute, Santa Fe, New Mexico 87501, USA

## ABSTRACT

**Removal of the 5′-leader region is an essential step in the maturation of tRNA molecules in all domains of life. This reaction is catalyzed by various RNase P activities, ranging from ribonucleoproteins with ribozyme activity to protein-only forms. In *Escherichia coli*, the efficiency of RNase P-mediated cleavage can be controlled by computationally designed riboswitch elements in a ligand-dependent way, where the 5′-leader sequence of a tRNA precursor is either sequestered in a hairpin structure or presented as a single-stranded region accessible for maturation. In the presented work, the regulatory potential of such artificial constructs is tested on different forms of eukaryotic RNase P enzymes—two protein-only RNase P enzymes (PRORP1 and PRORP2) from *Arabidopsis thaliana* and the ribonucleoprotein of *Homo sapiens*. The PRORP enzymes were analyzed in vitro as well as in vivo in a bacterial RNase P complementation system. We also tested in HEK293T cells whether the riboswitches remain functional with human nuclear RNase P. While the regulatory principle of the synthetic riboswitches applies for all tested RNase P enzymes, the results also show differences in the substrate requirements of the individual enzyme versions. Hence, such designed RNase P riboswitches represent a novel tool to investigate the impact of the structural composition of the 5′-leader on substrate recognition by different types of RNase P enzymes.**

**Keywords: synthetic riboswitches; tRNA 5′-processing; RNase P; PRORP; eukaryotes**

## INTRODUCTION

In the field of synthetic biology, riboswitch design represents a promising tool for customized and efficient regulation of gene expression. Riboswitches are *cis*-regulatory RNA elements, typically located in the 5′-untranslated region (5′-UTR) of a bacterial messenger RNA (mRNA) (Mironov et al. 2002; Nahvi et al. 2002; Winkler et al. 2002a,b; Serganov and Nudler 2013). Naturally occurring riboswitches control gene expression in a ligand-dependent manner, mostly at the level of transcription or translation. Their regulatory principle is based on two structural modules—an aptamer domain and an expression platform. The interaction of the ligand with the aptamer domain triggers a conformational rearrangement in the expression platform that—as a consequence—influences gene activity. The modular composition of riboswitches allows for the design of synthetic regulatory elements by the combination of such (natural or artificial) domains. Aptamers selected in vitro by systematic evolution of ligands by exponential enrichment (SELEX) are frequently used in this context (Ellington and Szostak 1990; Tuerk and Gold 1990). The well-characterized aptamer for theophylline is suitable for such designs, because it exhibits a high affinity to its ligand ($k_D$: 320 nM) and efficiently discriminates against molecules structurally related to theophylline, such as caffeine (Jenison et al. 1994; Zimmermann et al. 1997). In several approaches, it was successfully applied for the generation of synthetic riboswitches regulating translation or transcription (Fowler et al. 2008; Topp et al. 2010; Nakahira et al. 2013; Wachsmuth et al. 2013; Bueno et al. 2021). For the latter ones, computational

[6]These authors contributed equally to this work.
**Corresponding author: mario.moerl@uni-leipzig.de**
Article is online at http://www.rnajournal.org/cgi/doi/10.1261/rna.078814.121.

folding predictions were combined with experimental characterization by Wachsmuth et al. (2013, 2015). Based on the most efficient transcription regulating riboswitch from that work (RS10), new synthetic riboswitches were generated that control RNase P-dependent 5′-maturation of a tRNA (Ender et al. 2021).

In all organisms, tRNAs are synthesized as precursor transcripts that undergo a multistep maturation process until they can participate in translation (Phizicky and Hopper 2010; Hopper 2013; Shepherd and Ibba 2015). tRNA maturation includes removal of a 5′-leader and 3′-trailer, addition of the 3′-terminal CCA-end, specific modification of individual nucleosides, as well as splicing and aminoacylation (Schedl et al. 1976; Li and Deutscher 1996; Schürer et al. 2001; Lorenz et al. 2016). Whereas the details of most maturation steps vary in different organisms, cleavage of the 5′-leader is usually accomplished by RNase P (Kirsebom 2007; Klemm et al. 2016; Schencking et al. 2020), with minor exceptions (Randau et al. 2008). Throughout all domains of life, this enzyme exhibits a high structural diversity. In bacteria, RNase P consists of a small protein subunit (P protein) and an RNA moiety (P RNA), which represents the catalytically active subunit (Guerrier-Takada et al. 1983). In eukaryotes, the enzyme is of a higher complexity—for instance, human nuclear RNase P is composed of 10 protein subunits (hPOP5, RPP29, RPP30, RPP21, RPP38, hPOP1, RPP25, RPP20, RPP14, RPP40), and one RNA subunit (H1 RNA) (Jarrous 2002; Klemm et al. 2016). Besides such RNA-containing RNase P versions, protein-only RNase P enzymes were also discovered. In human mitochondria, the proteins MRPP1, MRPP2, and MRPP3 form a complex with tRNA 5′-processing activity (Holzmann et al. 2008; Walker and Engelke 2008). A protein-only RNase P (PRORP) consisting of a single protein moiety was identified in *Arabidopsis thaliana* (Gobert et al. 2010,2013). Today, after the identification of further PRORPs in *Aquifex aeolicus*, it is known that protein-only RNase P enzymes are present in all domains of life (Nickel et al. 2017; Daniels et al. 2019). Due to their diverse structural composition, the various types of RNase P show certain differences in substrate recognition. While several studies focus on the role of the tRNA 5′-leader sequence composition (Zahler et al. 2003, 2005; Sun et al. 2006; Niland et al. 2017), only very little information is available on the impact of its structural conformation. Several lines of experiments indicate that bacterial RNase P enzymes have an increased substrate affinity to unstructured 5′-leader regions (Lin et al. 2016; Niland et al. 2017; Ender et al. 2021). For other types of RNase P, the structural status of the leader region is postulated to be important as well (Lee et al. 1997; Ziehler et al. 2000; Brillante et al. 2016). In the case of *A. thaliana* PRORP3, it was shown that extensions of the tRNA acceptor stem can lead to cleavage at aberrant sites, and it was concluded that the flexibility of the 5′-leader near the cleavage position affects cleavage site selection (Brillante et al. 2016). However, there is no experimental evidence that the structural composition of the 5′-leader itself affects cleavage mediated by PRORP or eukaryotic nuclear RNase P enzymes.

The recently designed RNase P riboswitches (Ender et al. 2021) provide a tool to address this question. These riboswitches are based on the theophylline-binding aptamer (Jenison et al. 1994), where its 3′-part forms a sequester hairpin through interaction with a computationally designed sequence in the OFF state. This hairpin structure is directly followed by the regulated tRNA. Thus, the artificial 5′-leader is sterically masked in the hairpin structure in the absence of theophylline. Interaction with the ligand triggers opening of the sequester hairpin and the 5′-leader is converted into a single-stranded conformation, resulting in efficient RNase P-catalyzed tRNA-processing. Here, we analyzed the functionality of these riboswitches in the ligand-dependent control of tRNA maturation by eukaryotic RNase P enzymes, that is, in a new context. We show that the riboswitches can be used to examine tRNA processing by PRORP1 and PRORP2 from *A. thaliana* in vitro and in an RNase P complementation system in *Escherichia coli* according to Gößringer et al. (2017). Further, we replaced the tRNA fused to the riboswitch by $tRNA^{Pyl}$ from *Methanosarcina mazei* without losing ligand-dependent 5′-maturation, indicating that the riboswitch constructs can be applied to different tRNA species. The constructs fused to $tRNA^{Pyl}$ were then transferred into HEK293T cells to investigate their compatibility with human nuclear RNase P. The data presented here show that tRNA processing by PRORP as well as human nuclear RNase P can be influenced and controlled by the secondary structure of the 5′-leader region, confirming the assumption that 5′-leader accessibility is an important determinant for efficient processing not only by bacterial RNase P activities, but also by their eukaryotic counterparts (Brillante et al. 2016; Wu et al. 2018).

## RESULTS

In a previous study, we successfully generated RNase P riboswitch constructs through computational predictions (Ender et al. 2021). These riboswitches consist of the theophylline-dependent TCT8 aptamer (Jenison et al. 1994) overlapping with a designed expression platform (Fig. 1A). The constructs were fused at their 3′-end to suppressor $tRNA^{Tyr}$ (tRNA supF), and the 7 nt directly upstream of the tRNA were defined as the minimal 5′-leader region. In the absence of the ligand, this 5′-leader is masked through a sequester hairpin that—upon theophylline binding to the aptamer—unfolds into a single-stranded conformation. For this purpose, the in silico pipeline used included different structural constraints as the leader accessibility, the correct folding of the tRNA acceptor stem, and the independent folding of the riboswitch module and the

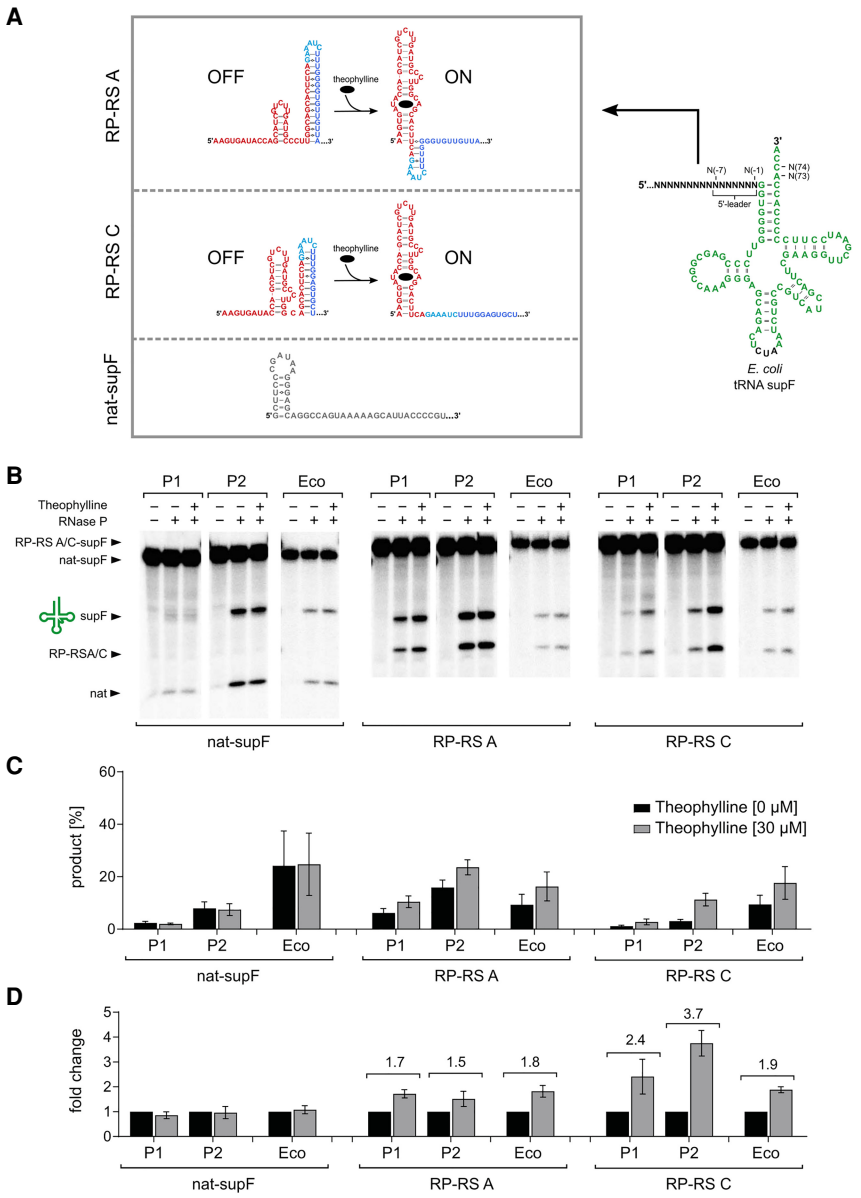


**FIGURE 1.** (*A*) Schematic representation of riboswitch and control constructs. The sequence of the theophylline aptamer is labeled in red, the hairpin loop region in cyan (taken from a transcription-regulating riboswitch construct [Wachsmuth et al. 2013; Ender et al. 2021]), and the complementary region forming the sequester hairpin in blue. The tRNA element is indicated in green (suppressor $tRNA^{Tyr}$ supF from *E. coli*). Base positions are numbered relative to the cleavage site and according to Sprinzl et al. (1998). The upstream sequence of the tRNA, represented as N stretch, is replaced by the respective 3′-part of each construct. Upon ligand binding (black oval), the riboswitch refolds, and the 5′-leader is no longer masked in the sequester hairpin and is accessible for cleavage. The natural leader sequence of the control construct nat-supF is indicated in gray. (*B*) In vitro analysis of riboswitch-controlled tRNA maturation. Cleavage of RP-RS A (*central* panel) and RP-RS C (*right* panel) by PRORP1 (P1), PRORP2 (P2), or *E. coli* RNase P holoenzyme (Eco) compared to supF with the naturally occurring 5′-leader (nat-supF; *left* panel) (Kirsebom and Svärd 1992). (*C*) Quantitation of the produced percentual product amount. Only in the case of RP-RS C, a theophylline-dependent tRNA processing is observed for all tested enzymes. Data are mean ± SD, $n = 4$. (*D*) Theophylline-induced fold changes of nat-supF (*left*), RP-RS A (*center*), and RP-RS C (*right*). Results show a low theophylline-dependent response ratio of 1.7- (PRORP1) and 1.5-fold (PRORP2) for RP-RS A and a clear activation for RP-RS C (PRORP1: 2.4-fold; PRORP2: 3.7-fold). Data are mean ± SD, $n = 4$.

tRNA (Ender et al. 2021). Normalized scores (with values between 0 and 1) based on predicted folding energies quantify to what extent each of these design goals is satisfied (Table 1). The synthetic riboswitches RP-RS A and RP-RS C efficiently regulate RNase P-mediated 5′-end processing of tRNA supF in *E. coli* (Ender et al. 2021). Here, these riboswitches were tested on different types of RNase P and the results indicate that they represent a valuable tool to get new insights into the structural requirements of the 5′-leader for processing by these maturation enzymes.

## Riboswitch RP-RS C causes theophylline-dependent activation of tRNA processing by PRORP1 and PRORP2

To examine whether RP-RS A and RP-RS C are also able to control processing by a protein-only RNase P enzyme, radioactively labeled in vitro transcripts of both constructs fused to tRNA supF were incubated in vitro with recombinant PRORP enzymes from *Arabidopsis thaliana* in the presence and absence of theophylline. Construct nat-supF consisting of tRNA supF with its native 43 nt long 5′-leader served as positive control (Kirsebom and Svärd 1992). PRORP1 and PRORP2 were used for the experimental examination, as they are well characterized, localized in different organelles, and differ in their substrate and temperature requirements (Brillante et al. 2016; Howard et al. 2016; Chen et al. 2019). The Hartmann group showed that PRORP1 is highly active at 37°C, while PRORP2 is completely inactive at this temperature and instead requires 28°C (Pavlova et al. 2012; Gößringer et al. 2017). Accordingly, these incubation temperatures were chosen for PRORP1 and PRORP2, respectively. In addition, enzyme and substrate concentrations were adjusted according to the described pre-tRNA affinities of PRORP1, PRORP2, and *E. coli* RNase P to avoid saturation effects in the

**TABLE 1.** In silico predictions of analyzed riboswitch constructs as previously described (Ender et al. 2021)

| Construct | | | | |
|---|---|---|---|---|
| ID | Switch length (nt) | Leader accessibility score | tRNA score | Independent fold score |
| **Riboswitches with tRNA supF** | | | | |
| RP-RS A | 63 | 0.484 | 0.992 | 0.932 |
| RP-RS C | 59 | 0.016 | 0.997 | 0.829 |
| **Riboswitches with hybrid tRNA supF** | | | | |
| RP-RS A-h | 63 | 0.480 | 0.995 | 0.935 |
| RP-RS C-h | 59 | 0.016 | 0.997 | 0.865 |
| **Riboswitches with $tRNA^{Pyl}$** | | | | |
| RP-RS A-P | 63 | 0.471 | 0.756 | 0.924 |
| RP-RS C-P | 59 | 0.012 | 0.999 | 0.874 |

The leader accessibility score measures how likely it is that a given construct implements the intended design model, that is, an accessible seven-nucleotide-long 5′-leader in the presence of theophylline and a masked 5′-leader in the absence of theophylline. The tRNA score and the independent fold score measure proper and independent folding of the tRNA sequence, respectively. Scores are only comparable for constructs of the same length. Sequences of each construct are summarized in Supplemental Table S1.

reactions. Howard et al. (2016) determined $k_M$ values for PRORP1 and PRORP2 in a range between 100 nM and 2 µM, depending on the pre-tRNA substrate. These values can only serve as a rough benchmark, as the riboswitch constructs represent artificial substrates that differ dramatically from native tRNA precursors. Thus, we chose 500 nM of tRNA substrate for PRORP1 and PRORP2 for this initial analysis, as a lower affinity than 100 nM was expected. Furthermore, we had to adjust the reaction buffer according to our previous RNase P riboswitch analysis to allow for a correct folding of the aptamer domain, which requires a concentration of $MgCl_2$ of at least 5 mM (Jenison et al. 1994; Ender et al. 2021). *E. coli* RNase P holoenzyme reaction served as positive control for theophylline-dependent tRNA processing. As *E. coli* RNase P has a much lower $K_M$ value for nat-supF (Ender et al. 2021), the tRNA substrate concentration was adjusted accordingly (50 nM). Cleavage reaction was induced by the addition of theophylline to a final concentration of 30 µM. Reaction products were separated on denaturing polyacrylamide gels and visualized by autoradiography. As shown in Figure 1B, all RNase P enzymes cleaved the tRNA substrates nat-supF, RP-RS A as well as RP-S C. Interestingly, PRORP1 shows a very low activity on nat-supF, which is probably caused by base-pairing of leader positions −1 and −2 with tRNA positions 73 and 74 (Kirsebom and Svärd 1992). A quantitative analysis of the relative amounts of released tRNA product was used to identify whether the enzymes show a ligand-dependent processing reaction (Fig. 1C). The large difference in the affinities of *E. coli* RNase P and the PRORP enzymes, respectively, required different enzyme and substrate concentrations. Cleavage efficiency therefore can be compared only between PRORP1 and PRORP2, for which identical substrate and enzyme concentrations were used. To compare the theophylline dependency of the processing reaction, ligand-induced fold changes were calculated for each enzyme (Fig. 1D). Cleavage of the positive control nat-supF by *E. coli* RNase P, PRORP1 as well as PRORP2 was not influenced by the addition of theophylline. For construct RP-RS A, a weak theophylline dependency of the tRNA maturation was observed. For PRORP1, tRNA release increased from 6.2 ± 1.7% (uninduced) to 10.4 ± 2.2% (induced), corresponding to a 1.7-fold change (Fig. 1C,D). A similar change of 1.5-fold was observed for PRORP2 with generally higher cleavage rates of 15.9 ± 2.8% and 23.6 ± 2.9%, as well as *E. coli* RNase P (9.3 ± 4.1% vs. 16.3 ± 5.5%, resulting in a 1.8-fold change). Construct RP-RS C seems to reduce PRORP-dependent processing especially in the absence of theophylline. In the case of PRORP1, only 1.1 ± 0.3% of background activity was observed, while the addition of the ligand led to 2.7 ± 1.1% product formation (2.4-fold activation) (Fig. 1C,D). PRORP2 revealed a 3.7-fold activation from 3.0 ± 0.7% to 11.3 ± 2.4% upon theophylline addition. For *E. coli* RNase P, cleavage of RP-RS C was comparable to RP-RS A (9.4 ± 3.5% vs. 17.6 ± 6.2%). Thus, RP-RS C exhibits in vitro a distinct theophylline-dependent tRNA maturation by all tested enzymes, although the overall efficiency in the case of PRORP1 is rather low.

## Multiple turnover kinetics with RP-RS A as a substrate indicate differences in PRORP1 and PRORP2 catalyzed cleavage

To gain deeper insights into the effect of the hairpin structure on affinity and catalysis, multiple turnover kinetics with both PRORP enzymes and RP-RS A construct were performed. Since the cleavage efficiency of the positive control nat-supF and RP-RS C was rather low in the initial single time point measurements (Fig. 1C), they were not used for

a kinetic examination, as this would have required an enormous amount of tRNA substrate that is not feasible due to the limited solubility of RNA (Tomita et al. 2004, 2006; Cho et al. 2005; Wende et al. 2015; Ernst et al. 2018; Pöhler et al. 2019). Interestingly, theophylline showed varying effects on the kinetic parameters depending on the type of enzyme. In the case of PRORP1, $k_{cat}$ was only slightly increased from 0.57 ± 0.11 $min^{-1}$ to 0.83 ± 0.06 $min^{-1}$ in the presence of theophylline, resulting in a change of 1.4-fold. The Michaelis–Menten constant showed no clear theophylline dependency (8.14 ± 2.84 µM vs. 6.4 ± 0.97 µM). For PRORP2, no theophylline dependency was observed regarding $k_{cat}$ (0.61 ± 0.07 $min^{-1}$ vs. 0.48 ± 0.04 $min^{-1}$). For this enzyme, a clear impact of theophylline on $k_M$ was visible (6.22 ± 1.37 µM vs. 1.93 ± 0.43 µM), leading to a 3.2-fold decrease. Taken together, while theophylline leads to higher cleavage efficiency for both enzymes, PRORP1 exhibits an impact on its reaction chemistry, while in PRORP2, substrate binding is affected by the structural composition of the 5′-leader.

## Riboswitch RP-RS C regulates PRORP-dependent processing in *E. coli* BW

To investigate ligand-dependent tRNA maturation under more physiological conditions, PRORP-catalyzed processing of RP-RS A and RP-RS C was analyzed in *E. coli* BW cells. A key feature of this strain is the chromosomal expression of the *rnpB* gene (coding for P RNA) under the control of promoter $P_{BAD}$, which can be induced by arabinose and repressed by glucose (Wegscheid and Hartmann 2006; Gößringer et al. 2017). PRORP enzymes were introduced on plasmid pDG148 (Gößringer et al. 2017) together with compatible pULTRA plasmids containing the riboswitch-tRNA constructs under a constitutively active proK promoter (Schultz et al. 2006). To compare tRNA maturation by the PRORP enzymes to the processing catalyzed by plasmid-encoded *E. coli* RNase P, a control plasmid pACYC carrying the *rnpB* gene was used according to Gößringer et al. (2017). For all constructs, tRNA maturation was monitored by northern blot analysis (Fig. 2A). As tRNA supF differs only in one nucleotide position from natural *E. coli* $tRNA^{Tyr}$, the use of a supF-specific probe is not possible. Thus, all constructs contained a hybrid tRNA supF-h, where anticodon stem and variable loop region of the tRNA were replaced by the corresponding parts of *Thermus thermophilus* $tRNA^{Tyr}$, leading to RP-RS A-h, RP-RS C-h, and nat-supF-h (Ender et al. 2021). For each construct, three individual clones were investigated. Interestingly, the individual clones exhibited rather strong differences in their growth rates, leading to incubation times between 3.5 and 23 h. These differences are likely the result of stochastic effects on transcription and

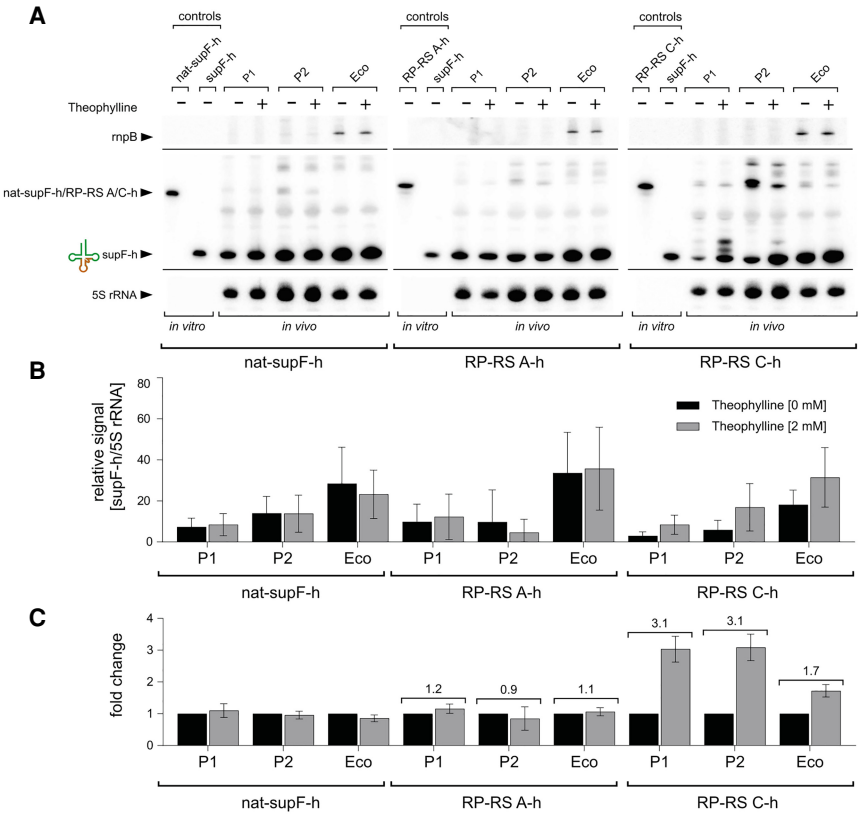


**FIGURE 2.** Riboswitch-controlled tRNA processing by PRORP enzymes in *E. coli* BW cells. (*A*) For the detection of processed tRNA, supF tRNA was replaced by a hybrid construct supF-h according to Ender et al. (2021). Northern blot analyses of plasmid-encoded constructs nat-supF-h, RP-RS A-h, and RP-RS C-h in *E. coli* BW cells with plasmids encoding genes for PRORP1 (P1), PRORP2 (P2), or the *E. coli* RNase P *rnpB* gene (Eco) are shown. A clear theophylline-dependent response was only visible for RP-RS C-h in combination with PRORP1 or PRORP2. In the case of RP-RS C-h in combination with PRORP1, further bands are visible, likely representing miscleaved precursor-tRNA fragments. (*B*) Relative quantitation of the mature tRNA. The corresponding hybridization signals were normalized to the signal of endogenous 5S rRNA. Only RP-RS C-h exhibits a theophylline-dependent response. The rather large error bars are the result of the variation of the absolute signal values between individual clones. Yet, all construct clones show an identical and reliable tendency of the influence of theophylline on mature tRNA supF-h release for each experiment (Supplemental Table S2). Data are mean ± SD, $n = 3$. (*C*) Theophylline-dependent fold changes of nat-supF-h, RP-RS A-h, and RP-RS C-h. For both PRORP1 as well as PRORP2, a clear theophylline-induced 3.1-fold response of RP-RS C-h was determined. The positive control Eco (*E. coli* RNase P) shows a 1.7-fold activation, corroborating the data of Ender et al. (2021). Data are mean ± SD, $n = 3$.

translation, described as gene expression noise (Paulsson 2004; Kaern et al. 2005; Kiviet et al. 2014; Kennard et al. 2016; Thomas et al. 2018). In addition, fluctuations of plasmid-based RNase P/PRORP expression can have further consequences, because the varying levels of enzyme activity affect the amount of processed tRNA. A high tRNA level can lead to saturation effects in the translation system, so that a nonnegligible fraction of the tRNAs will not be aminoacylated. Interaction of the uncharged tRNA with RelA then activates the stringent response, and a stress reaction is induced in the cell, which produces ppGpp, thereby affecting protein synthesis and, consequently, also cellular growth (Nazir and Harinarayanan 2016). This effect can be further enhanced by PRORP-catalyzed miscleavage, resulting in nonfunctional tRNA molecules that again trigger the stringent response (Trinquier et al. 2019).

For a comparative quantitation, the hybridization signals for the mature tRNA supF-h were calculated relative to the signal of endogenous 5S rRNA (Supplemental Table S2), indicating that only RP-RS C showed theophylline-dependent tRNA processing (Fig. 2B). While the absolute signal values of each clone showed a considerable variation, all clones of each individual construct exhibited the same influence of theophylline on the release of a mature tRNA supF-h (Supplemental Table S2). This becomes apparent when fold changes for all construct clones are calculated, as shown in Figure 2C. Similar to the positive control nat-supF-h, RP-RS A-h was processed by each of the three tested enzymes and showed no difference in the presence of theophylline (Fig. 2C). In contrast, RP-RS C-h exhibited a reduced processing in the absence of the ligand, resulting in a 3.1-fold change for PRORP1 and PRORP2, whereas *E. coli* RNase P showed a 1.7-fold activation upon theophylline addition. Interestingly, PRORP1, and to a certain degree also PRORP2, led to a considerable amount of miscleavage in combination with RP-RS C-h, as additional bands of somewhat lower electrophoretic mobility were detected in the presence of theophylline.

In some lanes of the gel, an additional band of lower electrophoretic mobility appeared, corresponding to a higher molecular weight compared to the unprocessed tRNA constructs. As identified by proteinase K treatment, these bands represent RNA–protein complexes that probably are the result of RelA binding to the tRNA precursor transcripts (Kushwaha et al. 2019; Ender et al. 2021). The correct expression or repression of plasmid-borne *E. coli* RNase P RNA subunit (*rnpB*) was verified using a specific probe addressing P RNA (Mohanty et al. 2020).

Taken together, only RP-RS C-h controlled tRNA processing by the PRORP enzymes in *E. coli* BW in a theophylline-dependent way, while RP-RS A-h showed a rather weak permanent ON state. The plasmid-encoded *E. coli* RNase P exhibited a similar behavior with 1.7-fold activation of RP-RS C-h and a ligand-independent ON state of RP-RS A-h. In our study on the endogenous RNase P in *E. coli* TOP10, both riboswitches showed an efficient ligand-dependent four- to fivefold activation (Ender et al. 2021). Thus, the here observed permanent ON state is obviously the result of the higher expression levels of P RNA due to the plasmid-encoded *rnpB* gene.

## Riboswitches RP-RS A-P and RP-RS C-P control tRNA$^{Pyl}$ maturation in *E. coli* TOP10

In a second line of experiments, we investigated whether RP-RS A and RP-RS C also regulate tRNA processing in human cells. To use a previously established reporter system in HEK293T cells for the analysis of tRNA maturation (Serfling et al. 2018), tRNA supF was replaced by tRNA$^{Pyl}$ from *M. mazei*, leading to constructs RP-RS A-P and RP-RS C-P. As the new tRNA sequence might interfere with the riboswitch element and hence cause misfolding, structure constraints from the in silico design were evaluated for the new tRNA in combination with the sequences of RP-RS A and RP-RS C (Table 1). Except for the lower tRNA score of RP-RS A-P that indicates the existence of alternative structures in the tRNA closing stem, all scores were in a range similar to the constructs containing tRNA supF. We then analyzed the secondary structures of the corresponding transcripts by in-line probing, and the results clearly support an independent folding of tRNA and riboswitch module (Fig. 3). For both riboswitches, the 5′-leader showed a pronounced single-stranded region in the presence of theophylline, comparable to riboswitches controlling tRNA supF maturation (Ender et al. 2021). In the ligand-bound state, positions N(−1) to N(−8) are single-stranded in RP-RS A-P, while in RP-RS C-P the whole leader is unfolded. Hence, these results indicate that the RNase P cleavage site should be accessible in both constructs when theophylline is bound. In addition, correctly folded aptamer and tRNA$^{Pyl}$ regions are visible in both constructs.

As the structure probing data indicate the intended theophylline-dependent structural rearrangement of the new riboswitch-tRNA fusions, we investigated their regulatory potential in *E. coli* TOP10 cells by northern blot according to Ender et al. (2021). For this purpose, both tRNA$^{Pyl}$-carrying constructs were inserted into plasmid pULTRA (Schultz et al. 2006) under control of a constitutively active proK promoter. le-tRNA$^{Pyl}$ served as positive control, representing a fusion of tRNA$^{Pyl}$ with the last 11 nt of the 5′-leader of RP-RS C. As this construct is lacking the whole aptamer element, the 11 nt leader region is not ligand-sensitive and should remain single-stranded regardless of the presence of theophylline. For both RP-RS A-P and RP-RS C-P, hybridization signals corresponding to a mature tRNA$^{Pyl}$ are visible, and the increased signal intensities in the presence of theophylline support a ligand-induced tRNA maturation (Fig. 4A). Quantitation of tRNA signals relative to 5S rRNA indicates a theophylline-induced threefold activation of RP-RS A-P ($0.4 \pm 0.16$ vs. $1.2 \pm 0.3$ relative signal

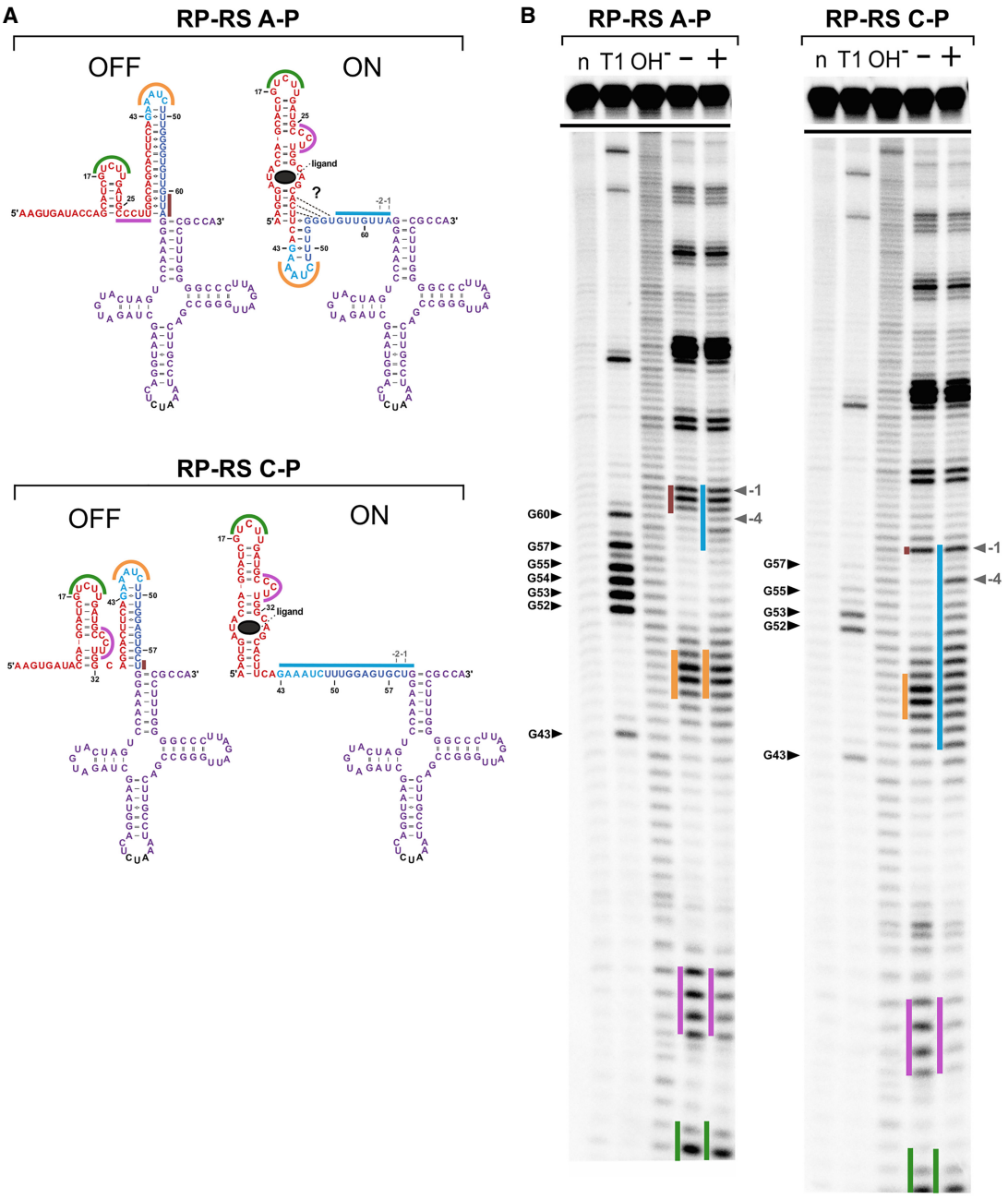


**FIGURE 3.** Secondary structure analysis by in-line probing. (*A*) Constructed secondary structures of ON and OFF states of riboswitches RP-RS A-P and RP-RS C-P fused to $tRNA^{Pyl}$. The theophylline-binding aptamer is presented in red, the hairpin loop region in cyan, the designed 3′-part of the sequester hairpin in blue, and $tRNA^{Pyl}$ in purple. The anticodon is shown in black. Bars in green, purple, orange, brown, and cyan represent regions identified as single-stranded in the corresponding structures. In the ON state of RP-RS A-h, additional possible interactions of the blue sequester part with the aptamer base are indicated by dashed lines and a question mark. (*B*) In-line probing patterns of riboswitch regions in RP-RS A-P and RP-RS C-P. Black horizontal lines in the two panels indicate a cut of the gel picture due to its length. Both constructs show a ligand-dependent opening of the sequester hairpin. In the uninduced state (absence of theophylline indicated by "−"), RP-RS A-P shows fraying of the basal three base pairs of the hairpin, supporting previous data on this construct (Ender et al. 2021). (n) Negative control (transcript without incubation), (T1) partial digest with RNase T1, ($OH^-$) alkaline hydrolysis, (−/+) incubation in in-line probing buffer for 40 h in the absence (−) or presence (+) of theophylline.

intensity), while RP-RS C-P exhibited a 14-fold induction due to a very low OFF state (0.1 ± 0.0 vs. 1.2 ± 0.4) (Fig. 4B). Similar to the results shown in Figure 2A, an additional slower migrating band is visible and likely represents an RNA–protein complex as previously identified by proteinase K treatment (Ender et al. 2021). Taken together, tRNA supF was successfully replaced by $tRNA^{Pyl}$ without losing theophylline-dependent switching activity of the

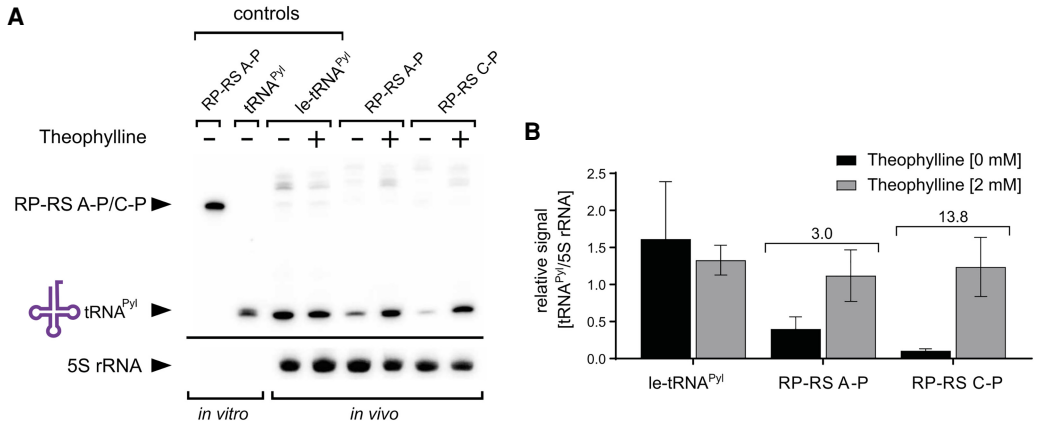


**FIGURE 4.** Riboswitch-controlled maturation of tRNA$^{Pyl}$ in *E. coli* TOP10 cells. (*A*) Northern blot analysis and (*B*) quantitation of tRNA$^{Pyl}$ hybridization signals normalized to the signal of the endogenous 5S rRNA. As positive control served le-tRNA$^{Pyl}$, a fusion of tRNA$^{Pyl}$ with the last 11 nt at of the 5′-end of RP-RS C. The additional band *above* the precursor signal (only clearly visible for the positive control le-tRNA$^{Pyl}$ and RP-RS A-P) likely represents a complex of processed, uncharged tRNA supF and protein RelA (Ender et al. 2021). In the calculated response ratios (*B*), RP-RS A-P showed a threefold theophylline-induced activation. For RP-RS C-P, the activation ratio was 13.8-fold. This increase is the result of a very low background cleavage in the absence of theophylline. Data are mean ± SD, $n = 3$.

regulatory platforms in RP-RS A and RP-RS C. Thus, both riboswitches with tRNA$^{Pyl}$ were further characterized for functionality in a human cell environment.

## Riboswitches RP-RS A-P and RP-RS C-P show theophylline-induced activation of tRNA$^{Pyl}$ in HEK293T cells

For the expression of riboswitches in HEK293T cells, sequences of RP-RS A and RP-RS C were inserted into plasmid pNEU upstream of a single copy of tRNA$^{Pyl}$ (Serfling et al. 2018). Transcription of these inserts was under control of a constitutively active U6 promoter. As described above, construct le-tRNA$^{Pyl}$ was used as a positive control. In addition to the riboswitch constructs, plasmid pNEU carries the open reading frame for an aminoacyl tRNA synthetase from *Methanosarcina barkeri* (MbPylRS$^{F}$, carrying mutation Y349F for efficient aminoacylation of tRNA$^{Pyl}$) (Serfling and Coin 2016). As the charged tRNA$^{Pyl}$ reads amber stop codons, its expression can be measured by suppression of a UAG stop codon in the mRNA of a reporter gene. Hence, a second plasmid derived from pcDNA 3.0 was introduced, carrying an *egfp* ORF with a corresponding stop codon at position 183. For the internal normalization of eGFP expression, this plasmid carries an additional ORF encoding for the mCherry protein (Serfling and Coin 2016; Serfling et al. 2018).

eGFP-dependent fluorescence resulting from riboswitch-controlled tRNA maturation was quantified and normalized to the mCherry fluorescence signal (as a value for transfection efficiency) (Serfling et al. 2018). Signals of the positive control le-tRNA$^{Pyl}$ (in the absence of theophylline) were set to 100% and used as a reference for quantitation of riboswitch-dependent signals (Fig. 5A). Addition of theophylline led to an unspecific decrease of the eGFP reference signal down to 66.6%. Northern blot analysis shows that this is the result of a reduction in tRNA$^{Pyl}$ expression (Fig. 5B,C). In the absence of the ligand, constructs RP-RS A-P and RP-RS C-P showed fluorescence signals comparable to negative control, which contains both pcDNA reporter plasmid as well as pNEU, where the U6 promoter required for tRNA$^{Pyl}$ expression was deleted. In the presence of the ligand, both riboswitch constructs exhibited a 2.0- to 2.3-fold activation (RP-RS A-P: 17.5 ± 2.3% vs. 34.8 ± 2.5%; RP-RS C-P: 8.6 ± 2.1% vs. 19.8 ± 2.4%) (Fig. 5A). Although the signal intensities were rather weak, these observations were confirmed by northern blot analysis, where the 5.8S rRNA hybridization signal was used for normalization (Fig. 5B,C; Serfling et al. 2018). In addition, the switching behavior of both riboswitches is corroborated in Figure 5D, where both constructs show a 1.9-fold change in tRNA$^{Pyl}$ maturation. In the autoradiogram shown in Figure 5B, a weak band migrating above the mature tRNA$^{Pyl}$ is visible. As the same band appears in northern blots from HEK cells without plasmids, this band represents a nonspecific signal not related to the riboswitch-regulated tRNA$^{Pyl}$ expression (data not shown). Interestingly, the positive control le-tRNA$^{Pyl}$ shows a higher expression level than the riboswitch constructs, which obviously is caused by structure and sequence composition of the riboswitch platforms (Fig. 5B).

Interestingly, in all constructs, tRNA maturation was rather inefficient, as a high amount of tRNA$^{Pyl}$ precursor is visible for positive control as well as riboswitch constructs (Fig. 5B). Yet, both RP-RS A-P and RP-RS C-P show a clear theophylline-dependent maturation of tRNA$^{Pyl}$ (and corresponding reporter gene expression), indicating that the structure of the 5′-leader region has an impact on human

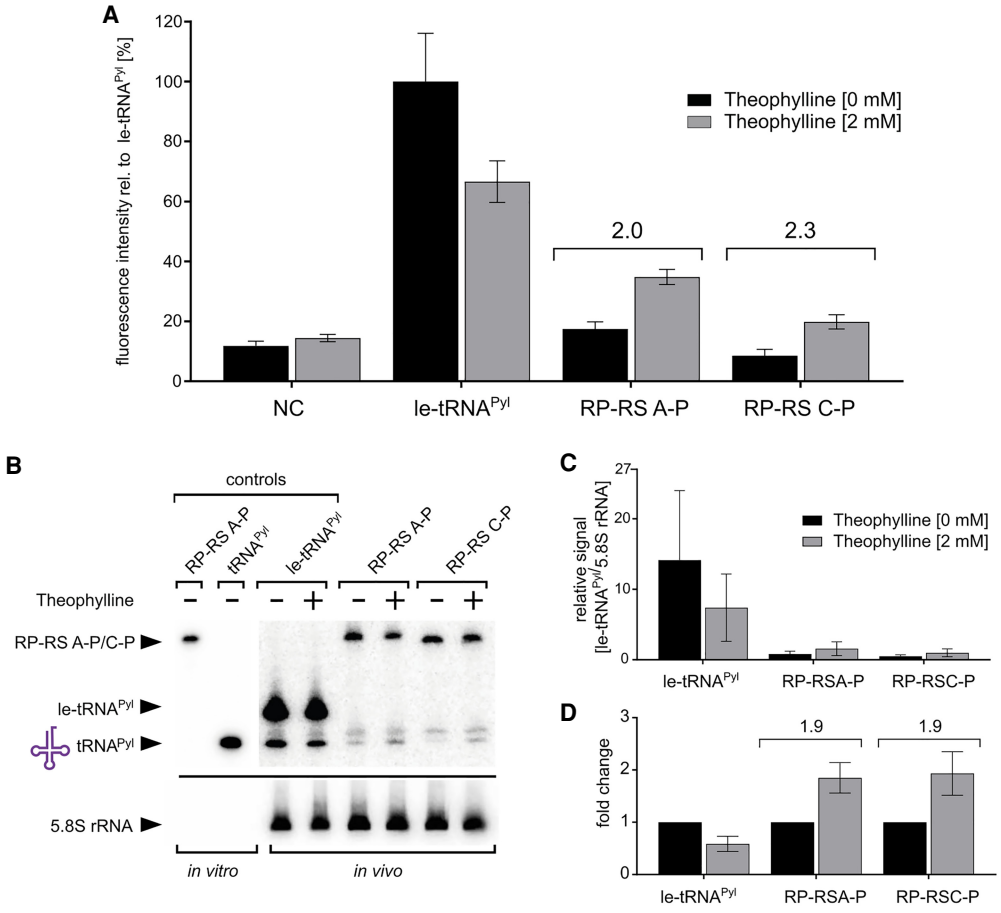


**FIGURE 5.** Riboswitch-controlled maturation of tRNA$^{Pyl}$ in HEK293T cells. (*A*) tRNA$^{Pyl}$-induced stop codon suppression at position 183 in the plasmid-encoded eGFP reporter mRNA led to a fluorescent signal that was used to monitor the switching behavior of the constructs. eGFP fluorescence intensities were normalized to the mCherry fluorescence signal derived from the *mcherry* ORF that was also encoded on the reporter plasmid and are presented relative to le-tRNA$^{Pyl}$. The fluorescence signal of the control le-tRNA$^{Pyl}$ shows a considerable reduction in the presence of the ligand, indicating a detrimental effect of theophylline on cell growth (Namba et al. 1980; Yasui and Komiyama 2001; Peng et al. 2018). Upon addition of the ligand, RP-RS A-P and RP-RS C-P show a twofold activation. Due to the negative growth effect of theophylline, this ratio is likely to be underrepresented. (NC) Negative control, tRNA$^{Pyl}$ without upstream-encoded U6 promoter. (*B*) Northern blot analysis and (*C*) quantitation of mature tRNA$^{Pyl}$ relative to the 5.8S rRNA signal. In agreement with the fluorescence data, the presence of theophylline leads to a reduction of mature tRNA$^{Pyl}$ in the case of le-tRNA$^{Pyl}$. However, theophylline-induced fold changes (*D*) show a twofold activation of both riboswitch constructs. Data are mean ± SD, $n = 3$.

RNase P-catalyzed tRNA maturation, comparable to PRORP and bacterial RNase P reactions. As theophylline shows an unspecific inhibitory effect on gene expression in HEK293T cells, the actual activation ratio of the riboswitches might be substantially higher.

## DISCUSSION

Recently, we showed that synthetic riboswitch constructs RP-RS A and RP-RS C control tRNA processing by *E. coli* RNase P in a ligand-dependent way by masking the 5′-leader of the tRNA precursor (Ender et al. 2021). These results corroborate the assumption that the conformation of the 5′-leader has an impact on RNase P-catalyzed tRNA 5′-maturation (Pomeranz Krummel et al. 2000; Lin et al. 2016; Niland et al. 2017). Here, we show that the same riboswitch constructs are useful tools to investigate the impact of the 5′-leader structure on tRNA processing by different types of RNase P from *A. thaliana* and *H. sapiens*. Most structure–function studies rely on mutational approaches, where the impact of individual base replacements on folding of the leader region and on the processing efficiency is investigated. Hence, not only the structure, but also the sequence of the leader region is affected, rendering an interpretation exclusively on the structural level rather difficult. In contrast, the riboswitch-based approach allows for a comparison that is solely based on structural differences, while the sequence of the leader per se remains unchanged, resulting in an unambiguous identification of structural effects on tRNA maturation. While our data represent a proof-of-concept for the design of RNase P riboswitches in eukaryotes, it is

impossible to give a benchmark for their functionality. Generally, a weak tRNA processing in the absence of the ligand is desired, as it reduces the background signal of the read-out system. On the other hand, a high activation range of tRNA expression and maturation can enhance the desired production of a certain protein (carrying for instance a nonproteinogenic amino acid), but it can also have a detrimental effect on the cells, if the produced tRNA is saturating components of the translational system such as aminoacyl-tRNA synthetases or elongation factors.

## PRORP1- and PRORP2-mediated tRNA processing can be regulated by riboswitch constructs

Compared to *E. coli* RNase P (Robertson et al. 1972), PRORP enzymes from *A. thaliana* were identified quite recently (Gobert et al. 2010). Accordingly, few data on substrate recognition are available for this type of activity. In addition, analysis of substrate recognition by PRORPs is more complex, as different substrate and reaction condition requirements for the three isoenzymes were identified (Gößringer et al. 2017; Chen et al. 2019). While *E. coli* RNase P recognizes part of the 5′-leader sequence, PRORP enzymes identify their substrates mainly based on the tRNA structure and position N(−1) (Brillante et al. 2016; Klemm et al. 2017). The riboswitch constructs corroborate these differences.

The in vitro data offer a first information about the impact of the 5′-leader structure on PRORP1 and PRORP2-mediated tRNA processing. As mentioned above, the theophylline-dependent percentual substrate formation has to be analyzed separately for *E. coli* RNase P, as other substrate and enzyme concentrations had to be chosen compared to the PRORP enzymes. The observation that PRORP2 showed a higher cleavage efficiency compared to PRORP1 is supported by the fact that the *Arabidopsis* PRORP enzymes cleave specific tRNA precursors with different efficiencies (Howard et al. 2016; Chen et al. 2019). Interestingly, the kinetic parameters of PRORP1 and PRORP2 acting on the most efficiently processed RP-RS A revealed differences in the theophylline-dependent regulation. For PRORP1, the presence of the ligand results in a slight 1.4-fold increase of $k_{cat}$. This is in agreement with the literature, where it is described that PRORP1 does not require a long accessible leader for efficient cleavage catalysis or substrate binding (Howard et al. 2016). The observed $k_M$ values in our study are higher compared to those for the cleavage of natural substrates. This is not surprising, as the artificial riboswitch constructs produce an unusually long and structured 5′-leader, which could negatively affect the substrate recognition. Furthermore, the reaction conditions differ from other studies, as they had to be adjusted to ensure an efficient ligand interaction of the theophylline aptamer. For example, Howard et al. (2016) used a buffer including 1 mM $MgCl_2$. However, when we tested our RNase P riboswitches in this buffer, no theophylline dependence of the PRORP-mediated cleavage was observed. It was shown that $MgCl_2$ is important for the correct folding of the aptamer and that a concentration below 5 mM $MgCl_2$ leads to a clear decrease of theophylline binding (Jenison et al. 1994). Thus, a compromise between PRORP enzyme functionality and aptamer folding/ligand binding had to be chosen to analyze riboswitch functionality. In contrast to PRORP1, PRORP2 showed a clear decrease of $k_M$ in the presence of theophylline (3.2-fold). While Howard et al. observed clear differences in $k_M$ values of individual pre-tRNAs for the different PRORP isozymes (Howard et al. 2016), a direct comparison to the riboswitch-carrying tRNA precursors is not possible. Further investigations of tRNA substrates with 5′-leaders varying in length and cleavage site accessibility, especially in combination with PRORP2, could provide more detailed information about the role of the 5′-leader accessibility.

While all enzymes efficiently processed RP-RS A, less mature tRNA was released from nat-supF (carrying the natural leader sequence) as well as RP-RS C. Prior studies showed that an interaction of leader position N(−1) with the usually unpaired tRNA discriminator base 73 (numbering according to Sprinzl et al. 1998) can lead to miscleavage and a decreased cleavage efficiency (Howard et al. 2016; Mao et al. 2016). Constructs nat-supF and RP-RS C carry a U(−1) residue that probably interacts with A(73) of the tRNA (Fig. 1A). Furthermore, in nat-supF, G(−2) can base pair with C(74), the first position of the tRNA CCA-end. Such acceptor stem interactions are not possible for RP-RS A, where the leader sequence ends with U(−2) and A(−1). Hence, cleavage of this construct is not affected. Support for this interpretation comes from in-line probing analysis of both riboswitch/supF constructs, where reduced hydrolysis at RP-RS C positions N(−1) to N(−3) indicate an involvement in base-pairing, even in the presence of theophylline (Ender et al. 2021). In contrast, the corresponding positions in RP-RS A showed an increased cleavage rate, supporting a single-stranded state.

The interaction of N(−1) and N(73) affects cleavage site selection by PRORP enzymes, provoking miscleavage of corresponding tRNA precursors (Howard et al. 2016). Additionally, this base-pairing also affects the cleavage efficiency, as it was shown by Mao et al. (2016). In agreement with this, RP-RS C, where U(−1) potentially interacts with the discriminator position A(73), reveals a reduced cleavage efficiency by PRORP1 and PRORP2 in vitro (Fig. 1B). In vivo, however, PRORP1, and to a certain degree also PRORP2, cause some miscleavage of RP-RS C-h, but not of nat-supF-h (Fig. 2A). The interaction of RNA-binding proteins with the tRNA in this and other tRNA precursor transcripts with large unstructured leader regions may stabilize the correct tRNA structure and, as a result, reduce miscleavage in vivo (Howard et al. 2016; Keffer-Wilkes et al. 2016).

In addition to the base-pairing status of N(−1) and tRNA position 73, the identity of N(−1) can also affect cleavage

efficiency. The Kirsebom laboratory demonstrated that PRORP enzymes prefer pre-tRNAs with A(−1) and G(−1) over substrates with U(−1) or C(−1) (Mao et al. 2016). However, such identities may not provoke miscleavage in every case, as 18.2% of the genomically encoded tRNA precursors include U(−1) and A(73) positions, but seem to be cleaved correctly (Mao et al. 2016). Yet, in artificial setups as the presented complementation system in *E. coli*, miscleavage due to the identity of N(−1) is conceivable. Nevertheless, both in vitro as well as in vivo (*E. coli* BW) data indicate that a theophylline-dependent control of tRNA maturation by PRORP enzymes is possible. In vitro, RP-RS A shows a certain regulatory effect on PRORP1, PRORP2, and the *E. coli* enzyme as a control (Fig. 1), while RP-RS C is more efficient with the protein-only enzyme versions (2.4- to 3.7-fold change; Fig. 1D). The activity of the *E. coli* enzyme with a 1.8- to 1.9-fold change corroborate our previous findings in a corresponding Michaelis–Menten kinetics analysis (Ender et al. 2021).

In the case of RP-RS C, both PRORP enzymes show a rather low background activity in the absence of theophylline, while the cleavage by the *E. coli* enzyme is much higher under these conditions (Fig. 1C). The bacterial RNase P interacts with the 5′-leader positions N(−1) to N(−8), whereas PRORP versions mainly interact with the tRNA structure and only with leader positions N(−1) and N(-2) (Brillante et al. 2016). For PRORP1, it was further shown that shortening the 5′-leader up to position N(−1) had no significant impact on the substrate affinity of the enzyme (Howard et al. 2016). Thus, the pronounced interaction of bacterial RNase P with the 5′-leader may facilitate the unfolding of the leader region even in the absence of theophylline, resulting in an increased background cleavage (Pomeranz Krummel et al. 2000). In vivo, the background of the endogenous (genomically encoded) RNase P is reduced, due to various factors such as fast degradation of unprocessed precursor tRNA (Li et al. 1998,2002), differences in enzyme and substrate concentrations and stabilization of tRNA precursor structures by RNA-binding proteins (Bilusic et al. 2014; Ender et al. 2021).

Such a less intense contact of PRORPs with the 5′-leader is further supported by the fact that RP-RS A shows only a low activation in vitro and no switching behavior in vivo. As positions N(−1) to N(−3) are already single-stranded in the OFF-state of RP-RS A (Ender et al. 2021), the cleavage site is obviously accessible for PRORP enzymes even in the absence of the ligand. In addition, the rather high expression level of the plasmid-encoded *PRORP* genes (Gößringer et al. 2017) could lead to a permanent ON state of this riboswitch in the cell. This hypothesis is supported by the fact that the combination of plasmid-encoded *rnpB* gene and RP-RS A also did not show a theophylline-dependent activation, while an in vivo study based on endogenous RNase P exhibited a fivefold activation for RP-RS A, as determined by northern blot analysis (Ender et al. 2021). Although *E. coli* RNase P presumably has a rather low affinity, the mere abundance of the overexpressed enzyme allows an efficient binding to RP-RS A even in the absence of theophylline, as N(−1) to N(−3) are unpaired and readily accessible for cleavage. In RP-RS C, the basis of the sequester hairpin is rather stable, as it consists of one A–U and two G–C base pairs, while the corresponding region in RP-RS A carries only one A–U and two G–U interactions (Fig. 3A). In addition, RP-RS C might form an additional base pair U(−1)-A73, further masking the cleavage site in the absence of the ligand. Due to these features, RNase P binding to the tRNA is not sufficient to unfold the leader region of RP-RS C, resulting in a theophylline-dependent tRNA processing. Hence, the increased accessibility of the RNase P cleavage site in the OFF state of RP-RS A renders its functionality obviously dependent on the enzyme concentration.

Taken together, all tested RNase P versions show a clear theophylline-dependent tRNA processing of RS-RP C in vitro as well as in vivo (Figs. 1D and 2C), demonstrating that the regulatory strategy of sequestering the 5′-cleavage site by hairpin formation is also valid for protein-only RNase P enzymes. Further, this observation shows that the accessibility of the first nucleotides of the 5′-leader has an impact on tRNA 5′-processing reactions not only of bacterial RNase P but also of PRORP enzymes (Brillante et al. 2016).

## Riboswitch-dependent tRNA processing by human nuclear RNase P

The transfer of bacterial riboswitch systems to mammalian cells is difficult, as the regulatory strategies differ considerably between pro- and eukaryotes. Most of the synthetic mammalian RNA-based switching systems use autocatalytic self-cleavage (aptazymes) to regulate gene expression, allowing quite efficient activation rates (Ausländer et al. 2010; Mustafina et al. 2020). Besides the aptazyme approach, our RNase P-regulating riboswitches reveal a new potential mechanism that might be functional in other domains of life as well.

The expression rates of the riboswitch constructs are rather low compared to the positive control le-tRNA$^{Pyl}$, indicating that highly structured leader regions might interfere with efficient transcription by RNA polymerase III. Furthermore, this polymerase terminates at stretches of U residues, and Orioli et al. (2011) showed that a minimum of two to three U residues is sufficient. In both riboswitch constructs, several of such U stretches are present (5x $U_2$, 1x $U_3$ in RP-RS A, 3x $U_2$, 1x $U_3$ RP-RS C) (Fig. 3A), and it is possible that these elements lead to premature transcription termination. In the higher expressed control le-tRNA$^{Pyl}$, the 11 nt leader region contains only a single $U_3$ stretch at its very 5′-end, rendering such termination rather unlikely. Moreover, maturation of tRNA$^{Pyl}$ is not very efficient in human cells, leading to an accumulation of unprocessed precursor transcripts as shown in Figure 5B. This low processing rate is

likely the result of more demanding substrate requirements of human RNase P compared to PRORPs or the *E. coli* enzyme. For instance, the structure of the TψC-arm, the variable loop and the anticodon loop have an impact on substrate recognition by eukaryotic RNA-based RNase P (Klemm et al. 2016). Additionally, the length of TψC-arm or acceptor stem has an impact on cleavage site selection, indicating that the eukaryotic enzyme follows a rather strict measuring procedure on its substrate (Yuan and Altman 1995; Hartmann et al. 2009; Klemm et al. 2016). The structure of $tRNA^{Pyl}$ from *M. mazei*, which was used in our experiments, exhibits several structural deviations from canonical human tRNAs. For example, it carries a smaller D-loop and a shorter variable loop (Serfling et al. 2018), that might lead to a reduced cleavage by nuclear RNase P. The resulting limitations of the heterologous $tRNA^{Pyl}$ expression and maturation can be overcome by using several copies of the corresponding tRNA expression cassette (Ryu and Schultz 2006; Serfling et al. 2018). The resulting increase in transcription leads to a certain, but not linear, increase in the production of a mature $tRNA^{Pyl}$. However, the produced pre-$tRNA^{Pyl}$ still represents a suboptimal substrate for human RNase P. A solution for this obstacle would be the optimization of the RNase P-recognition elements in $tRNA^{Pyl}$ without affecting its functionality, that is, the recognition elements for the corresponding pyrrolysyl-tRNA synthetase from *M. barkeri*. Alternatively, the riboswitch-controlled tRNA could be replaced by a version that is better adapted to tRNA maturation and functions in human cells. However, this will most likely require adjustments in the riboswitch sequence to exclude structural interference between the regulatory platform and the new tRNA (Ender et al. 2021). The independent fold score and the tRNA score are valuable predictive tools for this purpose. A further challenge for tRNA replacement is the fact that most eukaryotic tRNA sequences include intragenic type II RNA polymerase III promoters consisting of box A and B regions in D- and TψC-arm sequences (Galli et al. 1981). These promoters within the tRNA sequence interfere with riboswitch functionality, as they define a transcription start site located between 7 and 20 bp upstream of the box A element in the region encoding the tRNAs' D-arm (Schramm and Hernandez 2002; Orioli et al. 2012). As a consequence, the riboswitch elements with a length of 63 (RP-RS A) and 59 nt (RP-RS C) upstream of the tRNA sequence will not be completely transcribed, so that a ligand-dependent regulatory function is impossible. Hence, such RNase P riboswitches are strictly dependent on a type III promoter such as the U6 promoter used here, which consists only of upstream elements and lacks intragenic motives (Paule and White 2000). Only such promoter elements guarantee a fully transcribed upstream region of the tRNA, where the functional riboswitch is included.

In eukaryotes, regulation of tRNA expression remains challenging, as it is rather elaborate to convert an RNA polymerase III promoter into an inducible regulatory element (Henriksen et al. 2007). Thus, in most cases, constitutively active type III promoters such as H1 and U6 are used (Wang et al. 2007; Mukai et al. 2008; Serfling et al. 2018). The inducible riboswitch-dependent tRNA maturation might be especially useful in systems relying on orthogonal tRNA expression such as genetic code expansion, as it offers an additional option to regulate the production of a specific tRNA. Yet, the current switching efficiency of these elements has to be improved for such an application.

The ligand-dependent 5′-maturation of $tRNA^{Pyl}$ indicates that the leader accessibility has an impact on cleavage efficiency of human RNase P, supporting the observation that protein subunits of the corresponding yeast enzyme interact with the 5′-leader of its substrate, where the accessibility of the N(−1) position affects the cleavage rate (Lee et al. 1997; Lan et al. 2018). Taken together, our data demonstrate that designed riboswitches can regulate not only bacterial RNase P-mediated tRNA processing, but also affect the maturation catalyzed by the corresponding eukaryotic enzymes, by the RNA/protein assemblies or protein-only versions. Further, the results underline the applicability of these constructs to investigate the impact of the 5′-leader structure on the cleavage reaction of the various RNase P enzymes. The obtained information concerning the structural requirements of the 5′-leader region could improve the design of external guide sequences to efficiently induce RNase P-dependent cleavage of non-tRNA substrates such as pathogenic mRNA (Davies-Sala et al. 2015). Hence, such synthetic riboswitch designs do not only represent new regulatory modules in synthetic biology, but are valuable tools to shed light on the individual substrate requirements for the increasing number of different types of RNase P enzymes.

## MATERIALS AND METHODS

### Cloning of riboswitch-tRNA fusions

Riboswitch constructs were amplified from pBAD plasmids as previously described (Ender et al. 2021). PCR products of riboswitch modules or riboswitch-tRNA fusions were used for site directed mutagenesis to introduce the constructs into plasmids pULTRA-CNF (Schultz et al. 2006) or pNEU (Serfling et al. 2018).

### Cell culture and transfection

Cultivation and transfection of HEK293T cells (human embryonic kidney cells) were performed as previously described (Serfling et al. 2018) with minor deviations. $5 \times 10^5$ HEK293T cells were seeded per well on six-well plates in 2 mL complete growth medium. Transfection was performed after 1 d. For determination of eGFP expression, Lys(Boc) was added to the medium to a final concentration of 500 μM 1 h prior to transfection as described

(Serfling et al. 2018). This step was omitted in the direct detection of tRNA maturation by northern blots. Transfection was performed with 1 µg of the reporter plasmid (pcDNA3.0-eGFPY183TAG-mCherry) and 1 µg of plasmid pNEU (containing the riboswitch construct of interest), using polyethyleneimine 25 kDa (Polysciences). After 1 h of incubation, theophylline was added to a final concentration of 0 or 2 mM, representing a concentration that is well tolerated by the cells and that leads to an uptake sufficient enough for inducing ligand-dependent regulation in several riboswitches or aptazymes carrying the TCT8 aptamer (Wieland et al. 2009; Ausländer et al. 2010; Wachsmuth et al. 2013). Fluorescence assays or total RNA extractions for northern blots were performed 36 h after transfection.

## Fluorescence assay

Fluorescence assays were performed as previously described (Serfling et al. 2018). HEK293T cells were detached from the six-well plates 36 h after transfection by incubation with prewarmed 800 µL PBS/EDTA (PBS pH 7.4, 0.5 mM EDTA) at 37°C for 20 min. The suspension was transferred into a tube containing 200 µL PBS/$MgCl_2$ (PBS pH 7.4, 5 mM $MgCl_2$) followed by centrifugation for 2 min at 800*g* at room temperature (RT). The pellet was resuspended in 100 µL lysis buffer (50 mM Tris-HCl pH 8.0, 150 mM NaCl, 1% [v/v] Triton, 1 mM EDTA, 0.5 mM PMSF) followed by incubation for 30 min on ice with vigorous shaking every 5 min. The lysate was centrifuged for 10 min at 4°C and 14,000*g*. A total of 90 µL of the supernatant was used for fluorescence measurement in a dark 96-well plate (FLUOstar Omega, Filter eGFP: Ex485-12/Em520; filter mCherry: Ex584/Em620-10).

## Cultivation of *E. coli* TOP10 cells for total RNA isolation

Overnight cultures of *E. coli* TOP10 cells carrying pULTRA plasmids with the riboswitches fused to $tRNA^{Pyl}$ were grown in LB medium supplemented with 100 µg/mL spectinomycin. Cells were diluted to an OD600 of 0.06 in LB medium with 100 µg/mL spectinomycin and 0 or 2 mM theophylline. Cells were cultivated until OD600 of 0.5 was reached (around 3.5 h) and immediately used for total RNA isolation.

## Cultivation of *E. coli* BW cells for total RNA isolation

For the in vivo analysis of the cleavage by PRORP enzymes, *E. coli* BW cells (Wegscheid and Hartmann 2006; Gößringer et al. 2017) were used carrying plasmids pDG148 (encoding PRORP and $Amp^R$) and pULTRA (encoding a riboswitch construct of interest and $Spec^R$). Cells were cultivated as described with minor deviations (Gößringer et al. 2017). Precultures were grown in 3 mL LB medium supplemented with 100 µg/mL ampicillin, 35 µg/mL chloramphenicol, and 100 µg/mL spectinomycin for 6 h at 37°C. To induce chromosomal *rnpB* expression, arabinose was added to the LB medium to a final concentration of 10 mM. Cell pellets were washed two times with 3 mL LB medium supplemented with ampicillin, chloramphenicol, and spectinomycin and were diluted in 1 mL medium. This culture was used for inoculation of a 20 mL preculture in LB medium containing all three antibiotics and 10 mM glucose (to repress chromosomal *rnpB* expression) to OD600 of 0.01 and incubated for 14 h at 37°C (PRORP1, *E. coli* RNase P) or 28°C (PRORP2). The resulting overnight cultures were used to inoculate 5 mL LB medium with ampicillin, chloramphenicol, spectinomycin, glucose, and 0 or 2 mM theophylline. Cultures were incubated for 3.5–23 h at 37°C or 28°C. Total RNA was isolated at an OD600 of 0.5.

## Isolation of total RNA

RNA was isolated using TRIzol (Invitrogen). For HEK293T cells, medium was removed from the cells and 500 µL of TRIzol were added per well. Further isolation steps were performed according to the manufacturer. To isolate RNA from bacteria, 500 µL TRIzol were added to pellets from 2 × 5 mL cultures and resuspended. Afterward, 0.5 g zirconia beads were added to the suspension and cells were homogenized for 40 sec at 6 m/sec (FastPrep, Fisher Scientific). All further steps were performed according to the manufacturer. Isolated total RNA was dissolved in sterile water and stored at −20°C until use.

## Northern blot analysis

Northern blot experiments were performed as previously described (Ender et al. 2021). For the analysis of tRNA cleavage in *E. coli* cells, 9 µg of total RNA and 20 ng of in vitro transcript (control) were used. Probes for supF-h and 5S rRNA were used as previously described (Mohanty et al. 2012; Ender et al. 2021). Furthermore, another radioactively 5′-labeled DNA oligonucleotide with the sequence 5′-GGTTCTGTCGTGGACAGTC-3′ (Mohanty et al. 2020) was used to detect *rnpB* expression. For HEK293T cells, 12 µg of total RNA and 5 ng of in vitro transcript were used. DNA oligonucleotide probes for $tRNA^{Pyl}$ (5′-CGGA AACCCCGGGAATCTAACCCGGCTGAACGGA-3′) and 5.8S rRNA (5′-CGCAAGTGCGTTCGAAGTGTCGATGATCAATGTG-3′) were used according to Serfling et al. (2018).

## Expression and purification of *E. coli* RNase P and PRORP

Recombinant *E. coli* RNase P protein subunit was generated as previously described (Ender et al. 2021). Expression and purification of PRORP1 was performed according to Gößringer et al. (2017). Rosetta (DE3) pLYS RARE cells carrying plasmid pET28b_AtPRORP1 were grown in 4 × 300 ml LB medium with 50 µg/mL kanamycin and 35 µg/mL chloramphenicol at 37°C and shaking at 200 rpm. At an OD600 of 0.6, expression was induced by addition of IPTG to a final concentration of 1 mM. After 4 h of further incubation, cells were harvested as described (Ender et al. 2021). The resulting pellet was resuspended in 8 mL lysis buffer (50 mM Tris/HCl pH 7.4, 10% glycerol [v/v], 150 mM NaCl) and lysed (Ender et al. 2021). After centrifugation of the lysate at 4°C and 30,600*g* for 30 min, the supernatant was filtered (pore size 0.44 µm) and used for further purification. A HisTrap FF column (volume 1 mL) was preequilibrated with five column volumes (CVs) of 10% elution buffer (50 mM Tris/HCl pH 7.4; 10% glycerol [v/v], 150 mM NaCl, 500 mM imidazole) and 90% lysis buffer at a flow rate of 1 mL/min. The protein solution was

applied at a flow rate of 0.4 mL/min to the column on an ÄKTA pure system (Cytiva) and washed with 10 CV of 10% elution buffer and 90% lysis buffer followed by 3 CV 100% lysis buffer at a flow rate of 1 mL/min. Elution was performed using 5 CV of 100% elution buffer at the same flow rate. Protein-containing fractions were pooled and concentrated, and the final protein concentration was determined according to Bradford (1976). Glycerol was added to a final concentration of 40%, and 20 µL aliquots were frozen in liquid nitrogen and stored at −80°C.

Recombinant expression and purification of PRORP2 was performed as described (Gobert et al. 2010,2013) with deviations. Recombinant PRORP2 was expressed in *E. coli* BL21 (DE3) cells carrying plasmid pET28b_AtPRORP2 in 400 mL LB medium containing 50 µg/mL kanamycin at 37°C. At an OD600 of 1.5, additional 400 mL of cold LB medium (4°C) containing 50 µg/mL kanamycin and 2 mM IPTG were added, and cells were cultivated for 16 h at 16°C. Harvesting and disruption of cells by sonication were performed as previously described (Ender et al. 2021). For cell lysis, 5 mL of ice-cold lysis buffer (50 mM HEPES pH 7.5, 250 mM NaCl, 15% glycerol [v/v], 0.2 mM DTT, 5 mM imidazole) were used. The suspension was centrifuged for 30 min at 30,600*g* and 4°C. A HisTrap FF column (volume 1 mL) was preequilibrated using 5 CV of lysis buffer at a flow rate of 1 mL/min. Protein solution was loaded using a flow rate of 0.5 mL/min, followed by elution using 8 CV of elution buffer (50 mM HEPES pH 7.5, 250 mM NaCl, 15% glycerol [v/v], 0.2 mM DTT, 500 mM imidazole) without changing the flow rate. The protein solution was further purified by size exclusion chromatography on a HiLoad 16/600 Superdex 200 pg column in 30 mM HEPES pH 7.5, 150 mM NaCl, 5% glycerol (v/v), 0.2 mM DTT, and 5 mM $MgCl_2$. PRORP2-containing fractions were pooled, concentrated, and stored in 40% glycerol at −80°C.

## In vitro cleavage assays

In vitro cleavage assays were performed as described (Ender et al. 2021) with minor deviations. Radioactively labeled in vitro transcribed pre-tRNA substrate was mixed with reaction buffer (50 mM HEPES pH 7.6, 100 mM $NH_4Cl$, 10 mM $MgCl_2$) (Kazakov and Altman 1991), denatured in the absence or presence of theophylline for 1 min at 90°C and refolded for 5 min at room temperature. The cleavage reaction was started by the addition of RNase P enzymes. PRORP enzymes were added to final concentrations of 50 nM protein and 500 nM pre-tRNA substrate, and cleavage was performed at 37°C (PRORP1) or 28°C (PRORP2) for 3 min. *E. coli* RNase P holoenzyme was preincubated in reaction buffer at 37°C for 5 min with a 2:1 ratio of P protein and P RNA and was added to the substrate to final concentrations of 2 nM P RNA, 4 nM P protein, and 50 nM for the pre-tRNA transcript. Holoenzyme cleavage reaction was performed at 37°C for 3 min. All further steps were done as described (Ender et al. 2021). All in vitro cleavage assays were performed in at least three independent experiments.

## Multiple turnover kinetics for PRORP1 and PRORP2

Kinetic analysis of PRORP1 and PRORP2 were performed as described for the in vitro cleavage assays. A total of 200 nM PRORP1 or 150 nM PRORP2 was incubated with final substrate concentrations of 0.5–12 µM. The cleavage reaction was performed at optimal temperatures for PRORP1 (37°C) and PRORP2 (28°C) for 3 min. After separation by denaturing polyacrylamide gel electrophoresis, reaction products were quantified using ImageQuant TL 8.2. Michaelis–Menten parameters were determined using GraphPad PRISM (Ender et al. 2021). All cleavage assays for kinetic analysis were performed in at least three independent experiments.

## In vitro run-off transcription of riboswitch constructs and P RNA

In vitro transcripts were generated as described (Ender et al. 2021).

## Structure analysis of in vitro transcribed riboswitches

5′-labeled RNA was denatured at 90°C for 1 min and cooled down to room temperature for at least 5 min for refolding. In-line probing was performed as described (Regulski and Breaker 2008; Jühling et al. 2018; Ender et al. 2021) in the absence or presence of 30 µM theophylline for 40 h at room temperature in a 20 µL volume. Reactions were stopped by adding 20 µL of 2× colorless RNA loading dye (10 M urea, 1.5 mM EDTA), and 10 µL were loaded on a denaturing 10% PAA gel. Band patterns were visualized by autoradiography using a Typhoon PhosphorImager 9410 device (Cytiva).

## Quantitation and statistical analysis

For quantitation of in vitro cleavage assays and northern blots, autoradiograms were analyzed using the ImageQuant TL software (Cytiva). For in vitro cleavage assays, the background was determined as pixel intensity in the negative control at a position corresponding to the migration of the reaction product to be examined. The resulting value was subtracted from the respective band. The amount of mature tRNA was normalized by the sum of substrate and products. For northern blot quantitation, bands of mature tRNA were normalized to the signals of 5S rRNA in *E. coli* or 5.8S rRNA in HEK293T cells. Fold changes were calculated by the ratio of mature tRNA with theophylline to mature tRNA without theophylline. Statistical parameters and calculations are reported in the figures and figure legends.

## Calculation of design scores

In silico scores were calculated as described (Ender et al. 2021) using the hard- and soft-constraint framework of the ViennaRNA Package, version 2.4.11 (Lorenz et al. 2016). The leader accessibility score for a given sequence $x$ is

$$s_{accessibility}(x) = (1 - P(x|\Phi_{leader}))P(x|\Phi_{leader}, c_{ligand}),$$

where $P(x|\Phi_{leader})$ is the conditional probability that seven nucleotides of the leader sequence are unpaired and the $c_{ligand}$ term additionally refers to a bonus energy of 9.22 k cal $mol^{-1}$, added if a theophylline binding competent structure is formed. The tRNA score,

$$s_{tRNA}(x) = exp(-P(x|\Phi_{stem}, c_{ligand}) - P(x|\Phi_{stem})),$$

is again estimated using conditional probabilities but this time they constrain the ensemble of possible structures to those having a correctly folded tRNA closing stem. The independent fold score,

$$s_{indepfold}(x) = (G(x_{switch}) + G(x_{tRNA}))/G(x),$$

takes the sum of the ensemble-free energies of the riboswitch $G(x_{switch})$ and the tRNA $G(x_{tRNA})$ subsequences relative to the ensemble free energy $G(x)$ of the concatenated sequences. If both components fold independently this score becomes one.

## SUPPLEMENTAL MATERIAL

Supplemental material is available for this article.

## ACKNOWLEDGMENTS

We thank Roland Hartmann, Robert Serfling, and Giorgio Dieci for valuable discussions concerning PRORPs, $tRNA^{Pyl}$ usability, and RNA polymerase III termination. Special thanks goes to Irene Coin and her laboratory for providing laboratory access and expertise in cell culture and incorporation of nonnatural amino acids. We thank Roland Hartmann and Nadine Wäber for plasmids pDG148_PRORP1, pDG148_PRORP2, pET28b_PRORP1, and *E. coli* BW strain. We also thank Philippe Giegé for plasmid pET28b_PRORP2, Peter F. Schultz for plasmid pULTRA-CNF, Irene Coin for plasmids pcDNA3.0_eGFP183TAG_mCherry and pNEU-$tRNA^{Pyl}$, and Walter Rossmanith for donation of a recombinant PRORP1 preparation. This work was supported by the Deutsche Forschungsgemeinschaft (MO 634/9-2 to M.M. and STA 850/15-2 to P.F.S.).

*Received April 26, 2021; accepted December 21, 2021.*

## REFERENCES

Ausländer S, Ketzer P, Hartig JS. 2010. A ligand-dependent hammerhead ribozyme switch for controlling mammalian gene expression. *Mol Biosyst* **6:** 807–814. doi:10.1039/b923076a

Bilusic I, Popitsch N, Rescheneder P, Schroeder R, Lybecker M. 2014. Revisiting the coding potential of the *E. coli* genome through Hfq co-immunoprecipitation. *RNA Biol* **11:** 641–654. doi:10.4161/rna.29299

Bradford MM. 1976. A rapid and sensitive method for the quantitation of microgram quantities of protein utilizing the principle of protein-dye binding. *Anal Biochem* **72:** 248–254. doi:10.1016/0003-2697(76)90527-3

Brillante N, Gößringer M, Lindenhofer D, Toth U, Rossmanith W, Hartmann RK. 2016. Substrate recognition and cleavage-site selection by a single-subunit protein-only RNase P. *Nucleic Acids Res* **44:** 2323–2336. doi:10.1093/nar/gkw080

Bueno D, Pedrolli DB, Martins PMM, Bocchini DA, Moraes KCM, Facincani AP, Ferro JA, Varani AM, Pena MM, Ferreira H. 2021. Riboswitch theo/metE as a transcription regulation tool for *Xanthomonas citri* subsp. *citri*. *Microorganisms* **9:** 329. doi:10.3390/microorganisms9020329

Chen T-H, Sotomayor M, Gopalan V. 2019. Biochemical studies provide insights into the necessity for multiple *Arabidopsis thaliana* protein-only RNase P isoenzymes. *J Mol Biol* **431:** 615–624. doi:10.1016/j.jmb.2018.11.004

Cho HD, Verlinde CL, Weiner AM. 2005. Archaeal CCA-adding enzymes: central role of a highly conserved β-turn motif in RNA polymerization without translocation. *J Biol Chem* **280:** 9555–9566. doi:10.1074/jbc.M412594200

Daniels CJ, Lai LB, Chen T-H, Gopalan V. 2019. Both kinds of RNase P in all domains of life: surprises galore. *RNA* **25:** 286–291. doi:10.1261/rna.068379.118

Davies-Sala C, Soler-Bistué A, Bonomo RA, Zorreguieta A, Tolmasky ME. 2015. External guide sequence technology: a path to development of novel antimicrobial therapeutics. *Ann NY Acad Sci* **1354:** 98–110. doi:10.1111/nyas.12755

Ellington AD, Szostak JW. 1990. In vitro selection of RNA molecules that bind specific ligands. *Nature* **346:** 818–822. doi:10.1038/346818a0

Ender A, Etzel M, Hammer S, Findeiß S, Stadler P, Mörl M. 2021. Ligand-dependent tRNA processing by a rationally designed RNase P riboswitch. *Nucleic Acids Res* **49:** 1784–1800. doi:10.1093/nar/gkaa1282

Ernst FGM, Erber L, Sammler J, Jühling F, Betat H, Mörl M. 2018. Cold adaptation of tRNA nucleotidyltransferases: a tradeoff in activity, stability and fidelity. *RNA Biol* **15:** 144–155. doi:10.1080/15476286.2017.1391445

Fowler CC, Brown ED, Li Y. 2008. A FACS-based approach to engineering artificial riboswitches. *Chembiochem* **9:** 1906–1911. doi:10.1002/cbic.200700713

Galli G, Hofstetter H, Birnstiel ML. 1981. Two conserved sequence blocks within eukaryotic tRNA genes are major promoter elements. *Nature* **294:** 626–631. doi:10.1038/294626a0

Gobert A, Gutmann B, Taschner A, Gössringer M, Holzmann J, Hartmann RK, Rossmanith W, Giegé P. 2010. A single *Arabidopsis* organellar protein has RNase P activity. *Nat Struct Mol Biol* **17:** 740–744. doi:10.1038/nsmb.1812

Gobert A, Pinker F, Fuchsbauer O, Gutmann B, Boutin R, Roblin P, Sauter C, Giegé P. 2013. Structural insights into protein-only RNase P complexed with tRNA. *Nat Commun* **4:** 1353. doi:10.1038/ncomms2358

Gößringer M, Lechner M, Brillante N, Weber C, Rossmanith W, Hartmann RK. 2017. Protein-only RNase P function in *Escherichia coli*. Viability, processing defects and differences between PRORP isoenzymes. *Nucleic Acids Res* **45:** 7441–7454. doi:10.1093/nar/gkx405

Guerrier-Takada C, Gardiner K, Marsh T, Pace N, Altman S. 1983. The RNA moiety of ribonuclease P is the catalytic subunit of the enzyme. *Cell* **35:** 849–857.

Hartmann RK, Gößringer M, Späth B, Fischer S, Marchfelder A. 2009. The making of tRNAs and more: RNase P and tRNase Z. In *Molecular biology of RNA processing and decay in prokaryotes*, 1st ed. (ed. Condon C), pp. 319–368. Elsevier, Amsterdam.

Henriksen JR, Løkke C, Hammerø M, Geerts D, Versteeg R, Flaegstad T, Einvik C. 2007. Comparison of RNAi efficiency mediated by tetracycline-responsive H1 and U6 promoter variants in mammalian cell lines. *Nucleic Acids Res* **35:** e67. doi:10.1093/nar/gkm193

Holzmann J, Frank P, Loffler E, Bennett KL, Gerner C, Rossmanith W. 2008. RNase P without RNA: identification and functional reconstitution of the human mitochondrial tRNA processing enzyme. *Cell* **135:** 462–474. doi:10.1016/j.cell.2008.09.013

Hopper AK. 2013. Transfer RNA post-transcriptional processing, turnover, and subcellular dynamics in the yeast *Saccharomyces cerevisiae*. *Genetics* **194:** 43–67. doi:10.1534/genetics.112.147470

Howard MJ, Karasik A, Klemm BP, Mei C, Shanmuganathan A, Fierke CA, Koutmos M. 2016. Differential substrate recognition by isozymes of plant protein-only ribonuclease P. *RNA* **22:** 782–792. doi:10.1261/rna.055541.115

Jarrous N. 2002. Human ribonuclease P: subunits, function, and intranuclear localization. *RNA* **8:** 1–7. doi:10.1017/s1355838202011184

Jenison RD, Gill SC, Pardi A, Polisky B. 1994. High-resolution molecular discrimination by RNA. *Science* **263:** 1425–1429.

Jühling T, Duchardt-Ferner E, Bonin S, Wöhnert J, Pütz J, Florentz C, Betat H, Sauter C, Mörl M. 2018. Small but large enough: structural properties of armless mitochondrial tRNAs from the nematode *Romanomermis culicivorax*. *Nucleic Acids Res* **46:** 9170–9180. doi:10.1093/nar/gky593

Kaern M, Elston TC, Blake WJ, Collins JJ. 2005. Stochasticity in gene expression: from theories to phenotypes. *Nat Rev Genet* **6:** 451–464. doi:10.1038/nrg1615

Kazakov S, Altman S. 1991. Site-specific cleavage by metal ion cofactors and inhibitors of M1 RNA, the catalytic subunit of RNase P from *Escherichia coli*. *Proc Natl Acad Sci* **88:** 9193–9197. doi:10.1073/pnas.88.20.9193

Keffer-Wilkes LC, Veerareddygari GR, Kothe U. 2016. RNA modification enzyme TruB is a tRNA chaperone. *Proc Natl Acad Sci* **113:** 14306–14311. doi:10.1073/pnas.1607512113

Kennard AS, Osella M, Javer A, Grilli J, Nghe P, Tans SJ, Cicuta P, Cosentino Lagomarsino M. 2016. Individuality and universality in the growth-division laws of single *E. coli* cells. *Phys Rev E* **93:** 12408. doi:10.1103/PhysRevE.93.012408

Kirsebom LA. 2007. RNase P RNA mediated cleavage: substrate recognition and catalysis. *Biochimie* **89:** 1183–1194. doi:10.1016/j.biochi.2007.05.009

Kirsebom LA, Svärd SG. 1992. The kinetics and specificity of cleavage by RNase P is mainly dependent on the structure of the amino acid acceptor stem. *Nucleic Acids Res* **20:** 425–432.

Kiviet DJ, Nghe P, Walker N, Boulineau S, Sunderlikova V, Tans SJ. 2014. Stochasticity of metabolism and growth at the single-cell level. *Nature* **514:** 376–379. doi:10.1038/nature13582

Klemm BP, Wu N, Chen Y, Liu X, Kaitany KJ, Howard MJ, Fierke CA. 2016. The diversity of ribonuclease P. protein and RNA catalysts with analogous biological functions. *Biomolecules* **6:** 27. doi:10.3390/biom6020027

Klemm BP, Karasik A, Kaitany KJ, Shanmuganathan A, Henley MJ, Thelen AZ, Dewar AJL, Jackson ND, Koutmos M, Fierke CA. 2017. Molecular recognition of pre-tRNA by *Arabidopsis* protein-only ribonuclease P. *RNA* **23:** 1860–1873. doi:10.1261/rna.061457.117

Kushwaha GS, Bange G, Bhavesh NS. 2019. Interaction studies on bacterial stringent response protein RelA with uncharged tRNA provide evidence for its prerequisite complex for ribosome binding. *Curr Genet* **65:** 1173–1184. doi:10.1007/s00294-019-00966-y

Lan P, Tan M, Zhang Y, Niu S, Chen J, Shi S, Qiu S, Wang X, Peng X, Cai G, et al. 2018. Structural insight into precursor tRNA processing by yeast ribonuclease P, *Science* **362:** eaat6678 doi:10.1126/science.aat6678

Lee Y, Kindelberger DW, Lee JY, McClennen S, Chamberlain J, Engelke DR. 1997. Nuclear pre-tRNA terminal structure and RNase P recognition. *RNA* **3:** 175–185.

Li Z, Deutscher MP. 1996. Maturation pathways for *E. coli* tRNA precursors: a random multienzyme process *in vivo*. *Cell* **86:** 503–512. doi:10.1016/S0092-8674(00)80123-3

Li Z, Pandit S, Deutscher MP. 1998. Polyadenylation of stable RNA precursors in vivo. *Proc Natl Acad Sci* **95:** 12158–12162.

Li Z, Reimers S, Pandit S, Deutscher MP. 2002. RNA quality control: degradation of defective transfer RNA. *EMBO J* **21:** 1132–1138. doi:10.1093/emboj/21.5.1132

Lin H-C, Zhao J, Niland CN, Tran B, Jankowsky E, Harris ME. 2016. Analysis of the RNA binding specificity landscape of C5 protein reveals structure and sequence preferences that direct RNase P specificity. *Cell Chem Biol* **23:** 1271–1281. doi:10.1016/j.chembiol.2016.09.002

Lorenz R, Hofacker IL, Stadler PF. 2016. RNA folding with hard and soft constraints. *Algorithms Mol Biol* **11:** 8. doi:10.1186/s13015-016-0070-z

Mao G, Chen T-H, Srivastava AS, Kosek D, Biswas PK, Gopalan V, Kirsebom LA. 2016. Cleavage of model substrates by *Arabidopsis thaliana* PRORP1 reveals new insights into its substrate requirements. *PLoS ONE* **11:** e0160246. doi:10.1371/journal.pone.0160246

Mironov AS, Gusarov I, Rafikov R, Lopez LE, Shatalin K, Kreneva RA, Perumov DA, Nudler E. 2002. Sensing small molecules by nascent RNA: a mechanism to control transcription in bacteria. *Cell* **111:** 747–756.

Mohanty BK, Maples VF, Kushner SR. 2012. Polyadenylation helps regulate functional tRNA levels in *Escherichia coli*. *Nucleic Acids Res* **40:** 4589–4603. doi:10.1093/nar/gks006

Mohanty BK, Agrawal A, Kushner SR. 2020. Generation of pre-tRNAs from polycistronic operons is the essential function of RNase P in *Escherichia coli*. *Nucleic Acids Res* **48:** 2564–2578. doi:10.1093/nar/gkz1188

Mukai T, Kobayashi T, Hino N, Yanagisawa T, Sakamoto K, Yokoyama S. 2008. Adding l-lysine derivatives to the genetic code of mammalian cells with engineered pyrrolysyl-tRNA synthetases. *Biochem Biophys Res Commun* **371:** 818–822. doi:10.1016/j.bbrc.2008.04.164

Mustafina K, Fukunaga K, Yokobayashi Y. 2020. Design of mammalian ON-riboswitches based on tandemly fused aptamer and ribozyme. *ACS Synth Biol* **9:** 19–25. doi:10.1021/acssynbio.9b00371

Nahvi A, Sudarsan N, Ebert MS, Zou X, Brown KL, Breaker RR. 2002. Genetic control by a metabolite binding mRNA. *Chem Biol* **9:** 1043–1049. doi:10.1016/S1074-5521(02)00224-7

Nakahira Y, Ogawa A, Asano H, Oyama T, Tozawa Y. 2013. Theophylline-dependent riboswitch as a novel genetic tool for strict regulation of protein expression in Cyanobacterium *Synechococcus elongatus* PCC 7942. *Plant Cell Physiol* **54:** 1724–1735. doi:10.1093/pcp/pct115

Namba M, Nishitani K, Kimoto T. 1980. Effects of theophylline on the cell growth of normal and malignant human cells transformed in culture. *Gan* **71:** 621–627.

Nazir A, Harinarayanan R. 2016. (p)ppGpp and the bacterial cell cycle. *J Biosci* **41:** 277–282. doi:10.1007/s12038-016-9611-3

Nickel AI, Wäber NB, Gößringer M, Lechner M, Linne U, Toth U, Rossmanith W, Hartmann RK. 2017. Minimal and RNA-free RNase P in *Aquifex aeolicus*. *Proc Natl Acad Sci* **114:** 11121–11126. doi:10.1073/pnas.1707862114

Niland CN, Anderson DR, Jankowsky E, Harris ME. 2017. The contribution of the C5 protein subunit of *Escherichia coli* ribonuclease P to specificity for precursor tRNA is modulated by proximal 5′ leader sequences. *RNA* **23:** 1502–1511. doi:10.1261/rna.056408.116

Orioli A, Pascali C, Quartararo J, Diebel KW, Praz V, Romascano D, Percudani R, van Dyk LF, Hernandez N, Teichmann M, et al. 2011. Widespread occurrence of non-canonical transcription termination by human RNA polymerase III. *Nucleic Acids Res* **39:** 5499–5512. doi:10.1093/nar/gkr074

Orioli A, Pascali C, Pagano A, Teichmann M, Dieci G. 2012. RNA polymerase III transcription control elements: themes and variations. *Gene* **493:** 185–194. doi:10.1016/j.gene.2011.06.015

Paule MR, White RJ. 2000. Survey and summary: transcription by RNA polymerases I and III. *Nucleic Acids Res* **28:** 1283–1298. doi:10.1093/nar/28.6.1283

Paulsson J. 2004. Summing up the noise in gene networks. *Nature* **427:** 415–418. doi:10.1038/nature02257

Pavlova LV, Gössringer M, Weber C, Buzet A, Rossmanith W, Hartmann RK. 2012. tRNA processing by protein-only versus RNA-based RNase P: kinetic analysis reveals mechanistic differences. *Chembiochem* **13:** 2270–2276. doi:10.1002/cbic.201200434

Peng H, Su Q, Lin Z-C, Zhu X-H, Peng M-S, Lv Z-B. 2018. Potential suppressive effects of theophylline on human rectal cancer SW480

cells in vitro by inhibiting YKL-40 expression. *Oncol Lett* **15:** 7403–7408. doi:10.3892/ol.2018.8220

Phizicky EM, Hopper AK. 2010. tRNA biology charges to the front. *Genes Dev* **24:** 1832–1860. doi:10.1101/gad.1956510

Pöhler M-T, Roach TM, Betat H, Jackman JE, Mörl M. 2019. A temporal order in 5′- and 3′-processing of eukaryotic tRNAHis, *Int J Mol Sci* **20:** 1384 doi:10.3390/ijms20061384

Pomeranz Krummel DA, Kent O, MacMillan AM, Altman S. 2000. Evidence for helical unwinding of an RNA substrate by the RNA enzyme RNase P: use of an interstrand disulfide crosslink in substrate. *J Mol Biol* **295:** 1113–1118. doi:10.1006/jmbi.1999.3424

Randau L, Schröder I, Söll D. 2008. Life without RNase P. *Nature* **453:** 120–123. doi:10.1038/nature06833

Regulski EE, Breaker RR. 2008. In-line probing analysis of riboswitches. *Methods Mol Biol* **419:** 53–67. doi:10.1007/978-1-59745-033-1_4

Robertson HD, Altman S, Smith JD. 1972. Purification and properties of a specific *Escherichia coli* ribonuclease which cleaves a tyrosine transfer ribonucleic acid presursor. *J Biol Chem* **247:** 5243–5251.

Ryu Y, Schultz PG. 2006. Efficient incorporation of unnatural amino acids into proteins in *Escherichia coli*. *Nat Methods* **3:** 263–265. doi:10.1038/nmeth864

Schedl P, Roberts J, Primakoff P. 1976. In vitro processing of *E. coli* tRNA precursors. *Cell* **8:** 581–594. doi:10.1016/0092-8674(76)90226-9

Schencking I, Rossmanith W, Hartmann RK. 2020. Diversity and evolution of RNase P. In *Evolutionary biology—a transdisciplinary approach* (ed. Pontarotti P), pp. 255–299. Springer, Amsterdam.

Schramm L, Hernandez N. 2002. Recruitment of RNA polymerase III to its target promoters. *Genes Dev* **16:** 2593–2620. doi:10.1101/gad.1018902

Schultz KC, Supekova L, Ryu Y, Xie J, Perera R, Schultz PG. 2006. A genetically encoded infrared probe. *J Am Chem Soc* **128:** 13984–13985. doi:10.1021/ja0636690

Schürer H, Schiffer S, Marchfelder A, Mörl M. 2001. This is the end: processing, editing and repair at the tRNA 3′-terminus. *Biol Chem* **382:** 1147–1156. doi:10.1515/BC.2001.144

Serfling R, Coin I. 2016. Incorporation of unnatural amino acids into proteins expressed in mammalian cells. *Methods Enzymol* **580:** 89–107. doi:10.1016/bs.mie.2016.05.003

Serfling R, Lorenz C, Etzel M, Schicht G, Böttke T, Mörl M, Coin I. 2018. Designer tRNAs for efficient incorporation of non-canonical amino acids by the pyrrolysine system in mammalian cells. *Nucleic Acids Res* **46:** 1–10. doi:10.1093/nar/gkx1156

Serganov A, Nudler E. 2013. A decade of riboswitches. *Cell* **152:** 17–24. doi:10.1016/j.cell.2012.12.024

Shepherd J, Ibba M. 2015. Bacterial transfer RNAs. *FEMS Microbiol Rev* **39:** 280–300. doi:10.1093/femsre/fuv004

Sprinzl M, Horn C, Brown M, Ioudovitch A, Steinberg S. 1998. Compilation of tRNA sequences and sequences of tRNA genes. *Nucleic Acids Res* **26:** 148–153. doi:10.1093/nar/26.1.148

Sun L, Campbell FE, Zahler NH, Harris ME. 2006. Evidence that substrate-specific effects of C5 protein lead to uniformity in binding and catalysis by RNase P. *EMBO J* **25:** 3998–4007. doi:10.1038/sj.emboj.7601290

Thomas P, Terradot G, Danos V, Weiße AY. 2018. Sources, propagation and consequences of stochasticity in cellular growth. *Nat Commun* **9:** 4528. doi:10.1038/s41467-018-06912-9

Tomita K, Fukai S, Ishitani R, Ueda T, Takeuchi N, Vassylyev DG, Nureki O. 2004. Structural basis for template-independent RNA polymerization. *Nature* **430:** 700–704. doi:10.1038/nature02712

Tomita K, Ishitani R, Fukai S, Nureki O. 2006. Complete crystallographic analysis of the dynamics of CCA sequence addition. *Nature* **443:** 956–960. doi:10.1038/nature05204

Topp S, Reynoso CMK, Seeliger JC, Goldlust IS, Desai SK, Murat D, Shen A, Puri AW, Komeili A, Bertozzi CR, et al. 2010. Synthetic riboswitches that induce gene expression in diverse bacterial species. *Appl Environ Microbiol* **76:** 7881–7884. doi:10.1128/AEM.01537-10

Trinquier A, Ulmer JE, Gilet L, Figaro S, Hammann P, Kuhn L, Braun F, Condon C. 2019. tRNA maturation defects lead to inhibition of rRNA processing via synthesis of pppGpp. *Mol Cell* **74:** 1227–1238.e3. doi:10.1016/j.molcel.2019.03.030

Tuerk C, Gold L. 1990. Systematic evolution of ligands by exponential enrichment: RNA ligands to bacteriophage T4 DNA polymerase. *Science* **249:** 505–510.

Wachsmuth M, Findeiss S, Weissheimer N, Stadler PF, Mörl M. 2013. De novo design of a synthetic riboswitch that regulates transcription termination. *Nucleic Acids Res* **41:** 2541–2551. doi:10.1093/nar/gks1330

Wachsmuth M, Domin G, Lorenz R, Serfling R, Findeiss S, Stadler PF, Mörl M. 2015. Design criteria for synthetic riboswitches acting on transcription. *RNA Biol* **12:** 221–231. doi:10.1080/15476286.2015.1017235

Walker SC, Engelke DR. 2008. A protein-only RNase P in human mitochondria. *Cell* **135:** 412–414. doi:10.1016/j.cell.2008.10.010

Wang W, Takimoto JK, Louie GV, Baiga TJ, Noel JP, Lee K-F, Slesinger PA, Wang L. 2007. Genetically encoding unnatural amino acids for cellular and neuronal studies. *Nat Neurosci* **10:** 1063–1072. doi:10.1038/nn1932

Wegscheid B, Hartmann RK. 2006. The precursor tRNA 3′-CCA interaction with *Escherichia coli* RNase P RNA is essential for catalysis by RNase P in vivo. *RNA* **12:** 2135–2148. doi:10.1261/rna.188306

Wende S, Bonin S, Götze O, Betat H, Mörl M. 2015. The identity of the discriminator base has an impact on CCA addition. *Nucleic Acids Res* **43:** 5617–5629. doi:10.1093/nar/gkv471

Wieland M, Gfell M, Hartig JS. 2009. Expanded hammerhead ribozymes containing addressable three-way junctions. *RNA* **15:** 968–976. doi:10.1261/rna.1220309

Winkler W, Nahvi A, Breaker RR. 2002a. Thiamine derivatives bind messenger RNAs directly to regulate bacterial gene expression. *Nature* **419:** 952–956. doi:10.1038/nature01145

Winkler WC, Cohen-Chalamish S, Breaker RR. 2002b. An mRNA structure that controls gene expression by binding FMN. *Proc Natl Acad Sci* **99:** 15908–15913. doi:10.1073/pnas.212628899

Wu J, Niu S, Tan M, Huang C, Li M, Song Y, Wang Q, Chen J, Shi S, Lan P, et al. 2018. Cryo-EM structure of the human ribonuclease P holoenzyme. *Cell* **175:** 1393–1404.e11. doi:10.1016/j.cell.2018.10.003

Yasui K, Komiyama A. 2001. New clinical applications of xanthine derivatives: modulatory actions on leukocyte survival and function. *Int J Hematol* **73:** 87–92. doi:10.1007/BF02981908

Yuan Y, Altman S. 1995. Substrate recognition by human RNase P. Identification of small, model substrates for the enzyme. *EMBO J* **14:** 159–168.

Zahler NH, Christian EL, Harris ME. 2003. Recognition of the 5′ leader of pre-tRNA substrates by the active site of ribonuclease P. *RNA* **9:** 734–745. doi:10.1261/rna.5220703

Zahler NH, Sun L, Christian EL, Harris ME. 2005. The pre-tRNA nucleotide base and 2′-hydroxyl at N(-1) contribute to fidelity in tRNA processing by RNase P. *J Mol Biol* **345:** 969–985. doi:10.1016/j.jmb.2004.10.080

Ziehler WA, Day JJ, Fierke CA, Engelke DR. 2000. Effects of 5′ leader and 3′ trailer structures on pre-tRNA processing by nuclear RNase P. *Biochemistry* **39:** 9909–9916. doi:10.1021/bi000603n

Zimmermann GR, Jenison RD, Wick CL, Simorre JP, Pardi A. 1997. Interlocking structural motifs mediate molecular discrimination by a theophylline-binding RNA. *Nat Struct Biol* **4:** 644–649. doi:10.1038/nsb0897-644